UNIVERSITY OF BIRMINGHAM
University of Birmingham Research at Birmingham

Modelling photochemical pollutants in a deep urban street canyon: Application of a coupled two-box model approximation

Zhong, Jian; Cai, Xiaoming; Bloss, William

DOI:
10.1016/j.atmosenv.2016.08.027

License:
Creative Commons: Attribution-NonCommercial-NoDerivs (CC BY-NC-ND)

Document Version
Peer reviewed version

Citation for published version (Harvard):
Zhong, J, Cai, X & Bloss, W 2016, 'Modelling photochemical pollutants in a deep urban street canyon: Application of a coupled two-box model approximation', *Atmospheric Environment*, vol. 143, pp. 86-107. https://doi.org/10.1016/j.atmosenv.2016.08.027

Link to publication on Research at Birmingham portal

Publisher Rights Statement:
Checked for eligibility:12/08/2016

General rights
Unless a licence is specified above, all rights (including copyright and moral rights) in this document are retained by the authors and/or the copyright holders. The express permission of the copyright holder must be obtained for any use of this material other than for purposes permitted by law.

•Users may freely distribute the URL that is used to identify this publication.
•Users may download and/or print one copy of the publication from the University of Birmingham research portal for the purpose of private study or non-commercial research.
•User may use extracts from the document in line with the concept of 'fair dealing' under the Copyright, Designs and Patents Act 1988 (?)
•Users may not further distribute the material nor use it for the purposes of commercial gain.

Where a licence is displayed above, please note the terms and conditions of the licence govern your use of this document.

When citing, please reference the published version.

Take down policy
While the University of Birmingham exercises care and attention in making items available there are rare occasions when an item has been uploaded in error or has been deemed to be commercially or otherwise sensitive.

If you believe that this is the case for this document, please contact UBIRA@lists.bham.ac.uk providing details and we will remove access to the work immediately and investigate.

Download date: 24. Apr. 2024

Modelling photochemical pollutants in a deep urban street canyon: Application of a coupled two-box model approximation

Jian Zhong, Xiao-Ming Cai* and William James Bloss

School of Geography, Earth & Environmental Sciences, University of Birmingham, Edgbaston, Birmingham, B15 2TT, UK

**Corresponding author*. Tel.: (0121) 4145533; Fax: (0121) 4145528.

Email address: x.cai@bham.ac.uk (X.-M. Cai).

Abstract:

Air pollution associated with road transport is a major environmental issue in urban areas. Buildings in urban areas are the artificial obstacles to atmospheric flow and cause reduced ventilation for street canyons. For a deep street canyon, there is evidence of the formation of multiple segregated vortices, which generate flow regimes such that pollutants exhibit a significant contrast between these vortices. This results in poor air ventilation conditions at pedestrian level, thereby leading to elevated pollutant levels and potential breaches of air quality limits. The hypothesis of a well-mixed deep street canyon in the practical one-box model approach is shown to be inappropriate. This study implements a simplified simulation of the canyon volume: a coupled two-box model with a reduced chemical scheme to represent the key photochemical processes with timescales similar to and smaller than the turbulent mixing timescale. The two-box model captures the significant pollutant contrast between the lower and upper parts of a deep street canyon, particularly for NO_2. Core important parameters (i.e. heterogeneity coefficient, exchange velocity and box height ratio) in the two-box model approach were investigated through sensitivity tests. The two-box model results identify the emission regimes and the meteorological conditions under which NO_2 in the lower canyon (i.e. the region of interest for the assessment of human health effects) is in breach of air quality standards. Higher NO_2 levels were observed for the cases with higher heterogeneity

coefficients (the two boxes are more segregated), with lower exchange velocities (worse ventilation conditions), or with smaller box height ratios (reduced dilution possibly due to secondary smaller eddies in the lower canyon). The performance of a one-box model using the same chemical scheme is also evaluated against the two-box model. The one-box model was found to systematically underestimate NO_2 levels compared with those in the lower box of the two-box model for all the test scenarios. This underestimation generally tends to worsen for higher heterogeneity coefficients, lower exchange velocities or smaller box height ratios. This study highlights the limitation of the assumption of homogeneity in single box models for street canyon simulation, and the inherent uncertainties that must be borne in mind to appropriately interpret such model output (in particular, that a single-box treatment will systematically underestimate NO_2 as experienced at street level).

Keywords: Air pollution; Urban street canyon; Two-box model; Dynamics; Photochemistry.

1 Introduction

Air pollution associated with road transport is a major environmental issue in urban areas (Murena et al., 2009). A street canyon is a typical urban configuration with surrounding buildings along the street (Li et al., 2008). Buildings in urban areas are the artificial obstacles to urban atmospheric flow (Salim et al., 2011) and cause reduced ventilation for street canyons thereby leading to air pollution levels potentially much greater than air quality objectives (Sahm et al., 2002). The most fundamental geometrical model of an urban street is a single infinitely long street with buildings of the same height on both sides, normally termed as the two-dimensional (2D) idealised street canyon with perpendicular flow (Liu et al., 2011). The characteristics of recirculation in a 2D idealised street canyon are strongly dependent upon the canyon aspect ratio (*AR*), which is defined as the ratio of building height *H* to street width *W*. Under neutral meteorological conditions, the flow patterns can be classified into three regimes (Oke, 1987): isolated roughness (*AR*<0.3), wake interference (0.3<*AR*<0.7) and skimming flow (*AR*>0.7). Skimming flow representing the worst-case scenario for pollutant dispersion normally occurs in regular street canyons (0.7<*AR*<1.5) and deep street canyons (*AR*>1.5) (Murena et al., 2009). A single primary vortex is typically formed within regular street canyons (e.g. *AR*=1) (Baker et al., 2004). However, there is evidence of formation of multiple vortices within deep street canyons (e.g. Zhong et al. (2015); Li et al. (2009)), which can lead to greater contrasts in vertical pollutant distributions and create even poorer ventilation conditions for pollutants at the bottom of the canyon.

Many previous canyon modelling studies treated air pollutants as passive scalars (i.e. non-reactive pollutants) in street canyons as a first-order approximation. Caton et al. (2003) suggested three fundamental mechanisms that determine the concentration of a passive scalar in a 2D idealised street canyon, i.e. the emission rate, the advection-diffusion within the canyon, and the turbulent exchange (transfer) at the canyon roof level. For a practical application, the turbulent exchange mechanism is a major research challenge as this plays the key role in controlling the pollutant abundance in the street canyon (Barlow et al., 2004). This phenomenon can be represented by a

simplified parameter called ‘transfer velocity’ (Salizzoni et al., 2009) or ‘air ventilation rate’ (Liu and Leung, 2008), herein referred to as ‘exchange velocity’ (Bright et al., 2013), which is responsible for quantifying the exchange of mass between the street canyon and the overlying atmospheric boundary layer. However, many emissions from vehicles are reactive, evolving chemically as the air parcel is circulated inside the street canyon and exchanged with the air above the rooftop. Consequently, chemical processes, alongside dispersion and transport, are expected to play an important role in determining the abundance of reactive pollutants. Zhong et al. (2014) employed photochemical box models to investigate the segregation effects of heterogeneous emissions on ozone (O_3) levels in idealised urban street canyons and evaluate their uncertainty when grid-averaged emissions were adopted. Their study provides a simple and easy approach to consider the effects of both chemistry and dynamics using box models with a wide range of emission scenarios, but was restricted to idealised street canyons (completely segregated) with emission heterogeneity between them. Liu and Leung (2008) developed a one-box (chemistry) model to study reactive pollutant dispersion in street canyons (AR=0.5, 1, 2), using exchange velocity values derived from large-eddy simulations (LES) for different canyon ARs (Liu et al., 2005). Such models are unable to reproduce the significant contrasts of pollutant concentration between the lower and upper canyon regions, exacerbated in deep street canyons, since the whole canyon is treated as one well-mixed box for all ARs. Li et al. (2009) found that pollutants were at extremely high levels near the street level in deep street canyons. Field measurements in deep street canyons (Murena and Favale (2007); Murena et al. (2008)) also indicated that pollutant concentrations at pedestrian level in deep street canyons could be up to three times that in regular street canyons. Murena et al. (2011) and Murena (2012) attempted to implement a simplified two-box model (for passive scalars) with regard to the prediction of carbon monoxide (CO) concentrations in deep street canyons. The mass transfer between the two adjacent boxes inside the canyon is expressed by introducing an ‘exchange velocity’. Their study provided a useful guidance for improving the performance of the street-canyon operational models, e.g. Operational Street

Pollution Model (OSPM) (Buckland, 1998), which might otherwise be unreliable while applied into a deep street canyon since they were developed for street canyons with unity aspect ratio. CO in their two-box model was effectively considered a passive scalar (a reasonable approximation as CO has a long chemical lifetime (weeks) in the troposphere) and therefore no chemical processing was taken into account. Zhong et al. (2015) adopted a two-box model with the incorporation of simple NO_x-O_3 photochemistry, based on the existence of two vortices in a deep street canyon as characterised typical LES simulations. Their study enabled the consideration of reactive pollutants for the two-box model approach. However, only simple chemistry was considered, without the consideration of the volatile organic compounds (VOCs) processing (which may result in the additional conversion of nitric oxide (NO) to nitrogen dioxide (NO_2)) and production of O_3. Zhong et al. (2016) presented a comprehensive review of the recent numerical modelling studies that couple the dynamics and chemistry of reactive pollutants in urban street canyons. The computational fluid dynamics (CFD) modelling approach can provide high spatial and temporal resolution simulations of flow and pollutant fields within street canyons (e.g. Zhong et al. (2015); Bright et al. (2013); Kwak et al. (2013); Li et al. (2012)). However, they normally require a high level of computational resource and substantial input information (e.g. computational domain, flow characteristics, boundary conditions, and chemical schemes). As an alternative tool, the box model approach is relatively simple to use and permits relatively complex chemistry to be afforded in street canyon modelling such that it might provide a simpler tool to explore to air pollution issues for policy makers. Such box models normally require far less computational cost than CFD models. However, due to the inherent semi-empirical assumptions, box models are unable to reproduce the detailed distribution of the flow or pollutant fields in street canyons.

The two-box models of Murena et al. (2011) and Murena (2012) for an effective passive scalar or Zhong et al. (2015) with the simple NO_x-O_3 photochemistry have sucessfully captured the contrast between the bulk concentration in the lower street box and that in the upper street box. The present study will extend the coupled two-box model approach so that it considers both NO_x and VOCs

chemical processing under a variety of wind conditions for a wide range of emission scenarios, as a computationally efficient complement to (e.g.) full CFD simulations. The performance of a one-box model with the same chemical scheme will be evaluated compared with the more comprehensive two-box model. The methodology concerning the implementation of the two-box model with the complex chemistry is described in Section 2. Various factors affecting the performance of the two-box model are investigated and discussed in Section 3 and conclusions are presented in Section 4.

2 Framework of a coupled two-box model approximation

2.1 Model setup

In the box model approach, a well-mixed hypothesis is adopted, i.e. the air inside the box is assumed to be well-mixed. The box model is a simple approach to describe the evolution of air pollutants, which only requires low computational cost. For deep street canyons, the presence of two primary counter-rotating vortices segregates the street-canyon flow into layers with contrasting dynamical features so that pollutants exhibit a significant reduction with building height; this has been reported in the literature (Murena and Favale, 2007). In such situations, the "well-mixed" assumption tends to fail (Murena et al., 2011). Therefore, a more realistic model treatment (i.e. a two-box model) is needed to capture the vertically segregated layers with a significant concentration contrast and the communication between vortices in the deep street canyon. The deep street canyon can be divided into two boxes (conceptualised in Figure 1a) with the corresponding vortex inside each box separated by using a plane at the level of $z/H = \alpha$ (where a is the box height ratio determined by the flow structure with the street canyon). It is assumed that each vortex has sufficient intensity for the chemical species to be well-mixed within the corresponding box (Murena et al., 2011). The mathematical description of the two-box model is as follows:

$$\frac{dC_{i,L}}{dt} = -\frac{w_{t,L}}{H_L}(C_{i,L} - C_{i,U}) + E_{i,L} + \Delta S_{i,L} \quad (1)$$

$$\frac{dC_{i,U}}{dt} = \frac{w_{t,L}}{H_U}(C_{i,L} - C_{i,U}) - \frac{w_{t,U}}{H_U}(C_{i,U} - C_{i,b}) + \Delta S_{i,U} \quad (2)$$

where $C_{i,L}$ (ppb) and $C_{i,U}$ (ppb) are the concentrations of the i^{th} species in the lower and upper boxes, respectively; t (s) is the time; H_L (m) and H_U (m) are the heights of the lower and upper boxes, respectively; $w_{t,L}$ (m s^{-1}) is the exchange velocity between the lower and upper boxes, and $w_{t,U}$ (m s^{-1}) is the exchange velocity between the upper box and the overlying background atmosphere; $E_{i,L}$ (ppb s^{-1}) is the emission rates of the i^{th} species released from the lower canyon; $\Delta S_{i,L}$ (ppb s^{-1}) and $\Delta S_{i,U}$ (ppb s^{-1}) are the chemical source terms of the i^{th} species in the lower and upper boxes, respectively. A reduced chemical scheme (RCS), developed and validated by Bright et al. (2013), is adopted as the chemical mechanism in this study for the derivation of the chemical source terms to be used in Equations 1-2. The RCS includes 51 chemical species and 136 chemical reactions (Table A1 in the Appendix A). The two-box model approach without the consideration of chemistry (i.e. the chemical source terms in Equations 1-2 are zero and an effective passive (non-reactive) scalar is assumed) was initially developed and evaluated by Murena et al. (2011) and Murena (2012) based on the information from steady-state CFD simulations of deep street canyons. Subsequently, the two-box model approach considering simple NO_x-O_3 photochemistry (i.e. the chemical source terms in Equations 1-2 are derived from simple NO_x-O_3 photochemistry) was implemented by Zhong et al. (2015) based on the LES simulations of two vortices formed within a deep street canyon. These previous studies provide confidence that the simulated dynamics (exchange velocities) adopted for the street canyon boxes is reasonable although ideally such box models would be tested against observations (but these are as yet very scarce). This study attempts to extend the application of two-box model approach by considering relatively more complex chemistry (i.e. the RCS chemical mechanism).

The one-box model (with the "well-mixed" assumption for the whole deep street canyon) is conceptualised in Figure 1b and formulated below:

$$\frac{d}{dt}C_{i,0}(t) = E_{i,0} - \frac{w_{t,0}}{H_0}(C_{i,0} - C_{i,b}) + \Delta S_{i,0} \quad (3)$$

where the symbols are similar to those in the two-box model (the quantities associated are denoted as "0" rather than the "U" and "L" in the two-box model approach).

We assume that $C_{i,L}$ from the more sophisticated and realistic two-box model is the "true" value (in the sense that $C_{i,L}$ is closer to the true value in comparison with $C_{i,0}$ from the one-box model). Thus, there will be an error for the "one-box" model due to the well-mixed assumption, compared with the concentration in the lower box (i.e. the interest area of potential exposure assessment for pedestrians) by the "two-box" model. This error can be expressed as the concentration difference due to segregation as follows:

$$\Delta C_{i,L} = C_{i,0} - C_{i,L} \quad (4)$$

Then we can define the percentage of overestimation by the "one-box" model compared with the concentration in the lower box by the "two-box" model:

$$\phi_{i,L}(t) = \frac{\Delta C_{i,L}(t)}{C_{i,L}(t)} \times 100\% \quad (5)$$

If $\phi_{i,L}(t) = 0\%$, it means that the "one-box" model is in agreement with the "two-box" model; If $\phi_{i,L}(t) > 0\%$ or $\phi_{i,L}(t) < 0\%$, it means that the "one-box" model over- or under-estimates the concentration compared with the "two-box" model.

2.2 Exchange velocities in the two-box model

Exchange velocities implemented into the two-box model can be determined from a comprehensive numerical flow model (e.g. the Reynolds-Averaged Navier-Stokes model or large-eddy simulation) by calculating the ventilation of a passive scalar once the boundaries of the two boxes are defined. According to Fick's law, the flux of a passive scalar (denoted as "ps"), F_{ps} (ppb m s^{-1}), between

191 the lower and upper boxes under the steady state (the "two-box" model approach) can be written as
192 follows,

193 $$F_{ps} = w_{t,L}(C_{ps,L} - C_{ps,U}) \quad (6)$$

194 Similarly, the flux between the upper box and the background air under the steady state must be
195 equal to the flux in (6) and it can be expressed as:

196 $$F_{ps} = w_{t,U}(C_{ps,U} - C_{ps,b}) \quad (7)$$

197 If the whole street canyon is considered as one box, the flux of a passive scalar for the whole box
198 under the steady state (one-box model approach) is derived as:

199 $$F_{ps} = w_{t,0}(C_{ps,0} - C_{ps,b}) \quad (8)$$

200 We should also have the following equation due to the definitions of the three concentrations and
201 the volumes of the boxes:

202 $$C_{ps,0} = \alpha C_{ps,L} + (1-\alpha)C_{ps,U} \quad (9)$$

203 Equation 9 can be rewritten as:

204 $$C_{ps,0} = C_{ps,U} + \alpha(C_{ps,L} - C_{ps,U}) \quad (10)$$

205 Here, $\alpha \in (0,1)$ is the ratio of the lower box's volume to the volume of the whole canyon. When an
206 idealised street canyon is considered, α becomes the box height ratio, H_I/H_0. H_L can be determined
207 by the flow structure within the street canyon, namely, the height of the lower vortex.

208 In this study, it is assumed that $C_{ps,b} = 0$, i.e. 'zero background' is assumed for a passive scalar (e.g.
209 Murena et al. (2011) ; Murena (2012); Zhong et al. (2015)). According to Equations 7 and 8, it can
210 be derived that $\frac{w_{t,0}}{w_{t,U}} = \frac{C_{ps,U}}{C_{ps,0}}$, which denotes the ratio of the upper canyon concentration ($C_{ps,U}$) to

211 the whole canyon averaged concentration ($C_{ps,0}$) and represents the deviation from the homogenous
212 system (assuming the whole canyon as a well-mixed box). It is also assumed that $C_{ps,L} \geq C_{ps,U}$ is
213 the case for passive scalars emitted from street canyons near the ground level (Figure 2). According
214 to Equation 10, $C_{ps,0} \geq C_{ps,U}$ and $w_{t,0} \leq w_{t,U}$ can be derived. Then we may also define a non-
215 dimensional parameter to represent the heterogeneity coefficient (or spatial variation) across the two
216 boxes, i.e.

217 $$\eta = 1 - \frac{w_{t,0}}{w_{t,U}} \tag{11}$$

218 where $\eta \in [0,1]$. If $\eta = 0$, then $w_{t,0} = w_{t,U}$ from Equation **Error! Reference source not found.** and
219 it yields $C_{ps,0} = C_{ps,U}$ according to Equations 7 and 8, and $C_{ps,U} = C_{ps,L}$ based on Equation 10.
220 Thus, the two boxes are homogenous. Higher (or lower) values of η represent the two boxes that
221 are more (or less) segregated; in other words, the simulation possesses more (or less) heterogeneity.

222 According to Equations 6-9, it can be derived that:

223 $$\frac{1}{w_{t,0}} = \frac{\alpha}{w_{t,L}} + \frac{1}{w_{t,U}} \tag{12}$$

224 Based on Equations 6-12, exchange velocities for the two-box model are obtained as follows:

225 $$w_{t,U} = \frac{w_{t,0}}{(1-\eta)} \tag{13}$$

226 $$w_{t,L} = \frac{\alpha w_{t,0}}{\eta} \tag{14}$$

227 The physical mechanisms that determine the value of the heterogeneity coefficient (η) are explained
228 below. For a given α (i.e. fixed sizes of the two vortices), the heterogeneity coefficient may be
229 determined by the spatial pattern of turbulence, which could in turn be affected by the building

geometry, local wind conditions, local turbulence generated by moving vehicles or thermal forcing, and damped turbulence by (e.g.) tree leaf or stable atmosphere factors. For example, greater local vehicle generated turbulence (or other factors) transfers more pollutants from the lower box into the upper box, giving a lower value of $C_{ps,L}$ and a higher value of $C_{ps,U}$. Based on Equation 7, a lower value of $w_{t,U}$ is yielded. Then a lower value of η is obtained based on Equation **Error! Reference source not found.**; namely, the two-box system possesses less heterogeneity. If only the wind speed above the canyon is considered and the exchange velocity is assumed to be scaled with the wind speed (Murena et al. (2011) and Murena (2012)) for a given building geometry, η would remain unchanged (i.e. the ratio of exchange velocities in Equation 11 remains unchanged). Value of η may vary with the AR of the canyon, i.e. a larger AR (deeper canyon) may give a higher value of η due to the worse ventilation conditions. Also, lower turbulence caused by a stable atmosphere (Ramamurthy et al., 2007) and decoupling caused by an elevated tree-leaf canopy (Gromke and Ruck, 2012) may give higher values of η.

2.3 Model Scenarios

Table 1 gives an overview of the case settings. For the BASE case, these parameters are set as: $\eta = 0.5$, $w_{t,0} = 0.02$ m s^{-1} and $\alpha = 0.5$, which represent a typical urban scenario. The value of $\eta = 0.5$ represents a median level of heterogeneity, i.e. the pollutant concentration in the lower (or upper) box is 50% higher (or lower) than the mean concentration averaged over the whole canyon for a given a of 0.5. In other words, the concentration in the lower box is 3 times that in the upper box, which could be the case for deep street canyons (Murena and Favale (2007); Murena et al. (2008)). The value for $w_{t,0} = 0.02$ m s^{-1} is used based on those derived from large-eddy simulations for street canyons (e.g. Zhong et al. (2015); Bright et al. (2013)) while the reference incoming wind speed is about 2 m s^{-1}. This investigation is focused on highly polluted scenarios, i.e. calm wind blowing across the street canyon rather than windy conditions. $w_{t,0}$ is assumed to scale with the reference wind speed above the street canyon (Murena et al. (2011) and Murena (2012)) while

keeping the same turbulence pattern. The value of $\alpha = 0.5$ represents equal size vortices (volume of air) for both lower and upper boxes (e.g. found in the CFD study by Kwak et al. (2013)), which represents a typical situation for deep street canyons. To investigate the effect of η, the values of other parameters are assumed to kept the same as those used in Case BASE and a series of values of η are considered, i.e. Case HC-LL ($h = 0.1$), Case HC-L ($\eta = 0.3$), Case HC-H ($\eta = 0.7$) and Case HC-HH ($\eta = 0.9$). Likewise, a series of other cases together with their parameters are also summarised in Table 1, i.e. the effect of varying $w_{t,0}$ with Case EX-LL ($w_{t,0}$ =0.012 m s^{-1}), Case EX-L ($w_{t,0}$ =0.016 m s^{-1}), Case EX-H ($w_{t,0}$ =0.024 m s^{-1}) and Case EX-HH ($w_{t,0}$ =0.028 m s^{-1}); and the effect of varying a with Case HB-LL ($a = 0.1$), Case HB-L ($a = 0.3$), Case HB-H ($a = 0.7$), and Case HB-HH ($a = 0.9$). As both η and α range from 0 to 1, our tests of (0.1, 0.9) for both parameters covers a wide range of most possible scenarios. Our tests of (0.012, 0.028) m s^{-1} for the exchange velocity are mainly focus on the sensitivity to this typical situation (0.02 m s^{-1} for Case BASE). For each case, the corresponding 'one-box' model and the 'two-box' model were run (Figure 1). Figure 3 illustrated the exchange velocities (based on Equations 13-14) implemented in the 'two-box' model for the scenarios in Table 1, considering the effect of η, $w_{t,0}$ and a, respectively. Figure 3a shows that, for a given $\alpha = 0.5$ and $w_{t,0} = 0.02$ m s^{-1}, as η increases, $w_{t,L}$ increases, but $w_{t,U}$ decreases. Figure 3b shows that, for a given $\alpha = 0.5$ and $\eta = 0.5$, as $w_{t,0}$ increases, both $w_{t,L}$ and $w_{t,U}$ increases linearly. This linear relationship is also found in the literature (Murena et al., 2011). Figure 3c shows that, for a given $\eta = 0.5$ and $w_{t,0} = 0.02$ (m s^{-1}), as α increases, $w_{t,L}$ remains the same level, but $w_{t,U}$ increases linearly.

For each case (listed in Table 1), the corresponding 'one-box' model and the 'two-box' model were run (Figure 1). Initial and background conditions of chemistry used in this study follow those of Zhong et al. (2014), in which the independent photochemical box model is initially spun up to allow concentrations of all 51 species in RCS to be calculated. In order to characterise a wide range of

real scenarios, the representative E_{NOx} and E_{VOCs} are scaled by different factors of between 0.1 and 2 applied to those of the "Typical Real-world Emission Scenario" (TRES) (i.e. 620, 128 and 1356 g km^{-1} hr^{-1} for emission rates for NO_x, VOCs and CO, respectively) (Zhong et al., 2014), which represents an urban continuous road traffic of 1500 vehicles h^{-1} with an average speed of 30 mph and a vehicle fleet composition for the UK in the year 2010.

The lower street canyon is the volume of interest for the assessment of human health effects (i.e. where exposure occurs). NO_2 is an important photochemical pollutant and the issue of NO_2 air pollution has become an urgent agenda for the urban air quality management (Defra, 2015). This article will focus on the effects of η (heterogeneity coefficient) and $w_{t,0}$ (exchange velocity), and α (box height ratio) on the NO_2 characteristics in the lower canyon (box), once photochemical box models have reached a quasi-steady state. The coupled two-box model represents the key photochemical processes with timescales similar to and smaller than the turbulent mixing timescale in street canyons. The typical time scale for the street canyon air to exchange with the external flow aloft is $H_0 / w_{t,0}$, which is an order of 10 min (Bright et al. (2013)). Although the chemistry system is complex and highly nonlinear, possessing a wide range of chemical time scales, the box model will eventually achieve a quasi-steady state (pollutants remain nearly constants) as the run time is much larger than the exchange timescale, leaving those slow chemical reactions still slightly 'unsteady' (Bright et al. (2013)).

3 Results and discussion

3.1 Effect of the heterogeneity coefficient

Figure 4 illustrates the effect of the heterogeneity coefficient (η) on $C_{NO_2,L}$ (ppb), i.e. the NO_2 concentration in the lower box, for (a) Case HC-LL (η=0.1), (b) Case HC-L (η=0.3), (c) Case BASE (η=0.5), (d) Case HC-H (η=0.7), (e) Case HC-HH (η=0.9) and (f) Selected lines for analysis. In Figure 4, E_{VOCs} and E_{NOx} are normalised to the corresponding values in the "Typical

303 Real-world Emission Scenario" (TRES, represented by △), derived from the fleet composition for
304 the year 2010. The trajectory 2005-2020 shown in Figure 4 (line on each panel) represents the
305 changing emission scenarios for 2005 to 2020, derived from the UK fleet composition projections
306 (NAEI, 2003) and the UK Road Vehicle Emission Factors (Boulter et al., 2009) assuming constant
307 traffic volumes and speeds equal to those in the 'TRES' scenario for 2010 - i.e. only the emission
308 change with vehicle technology and fleet composition is considered, rather than traffic growth. The
309 solid red curves highlight the UK air quality standard for hourly NO_2 (105 ppb) (no exceedances
310 more than 18 times a year) (Defra, 2008). It is interesting to note that $C_{NO_2,L}$ generally has a similar
311 pattern for the cases and increases with the heterogeneity coefficient from 0.1 (Figure 4a) to 0.9
312 (Figure 4e). This can be explained by the reducing exchange between the lower and upper box
313 (indicated by a lower value of $w_{t,L}$ when η is large in Figure 3a). The higher heterogeneity
314 coefficient may also be considered to reflect less local traffic produced turbulence in the lower box,
315 as this would reduce the air ventilation from the lower box to the upper box. This is consistent with
316 the finding by Murena et al. (2011) that there would be a lower exchange velocity between the
317 lower and upper box and a higher level of pollutant concentration in the lower box for the case
318 without considering the local traffic produced turbulence. This indicates that heterogeneity in the
319 street canyon significantly affects pollutant concentrations in the lower box. Therefore, it is not
320 surprising that the solid red curve shifts from the higher emission region to the lower emission
321 region as the heterogeneity coefficient increases (Figure 4a-e). The curve shift (or more generally,
322 the pattern shift) is not linear, mainly due to the highly non-linear chemical regimes. It is also noted
323 that emissions at the TRES level are expected to lead to NO_2 concentrations in breach of the UK air
324 quality standard for hourly NO_2, for this idealised scenario, while the heterogeneity coefficient is
325 larger than 0.5 (Figure 4c-e). It is observed that trajectory 2005-2020 cuts across the solid red curve.
326 This indicates the importance of future technology in the expected reduction of NO_2 levels thereby
327 meeting the UK NO_2 air quality standards over years (although we note that such anticipated
328 reduction may not be fully realised (Carslaw and Rhys-Tyler, 2013)). For a heterogeneity

coefficient of 0.9, the UK air quality standard for hourly NO_2 is breached for most years, for this idealised scenario. This indicates that it is important to improve the air ventilation within the street canyon, thereby decreasing the heterogeneity coefficient leading to better air quality and reduced pedestrian exposure.

Figure 5 shows the transects of $C_{NO_2,L}$ (ppb) for Case HC-LL, Case HC-L, Case BASE, Case HC-H and Case HC-HH through the selected lines for analysis in Figure 4f. The dashed line in Figure 4f ("Fixed E_{NOx}") represents a technology change targeting only E_{VOCs} from vehicles, or roads with a varying coverage of vegetation which may emit further VOCs into the urban canopy (Loughner et al., 2012). The dotted line in Figure 4f ("Fixed E_{VOCs}") represents a technology change targeting only E_{NOx} from vehicles. The dot-dash line in Figure 4f ("TRES-2010") represents a technology of both E_{VOCs} and E_{NOx} with the proportional change in traffic emissions of both VOCs and NO_x from vehicles specified for the TRES. This dot-dashed line may also represent control of the number of vehicles in streets or scenarios for different areas (busier or less busy roads) with the same fleet composition as the TRES. The trajectory line ("Trajectory 2005-2020") indicates emission scenarios for the years 2005 to 2020 with the same traffic volume and speed as the TRES. The corresponding results along the selected lines are analysed below.

Figure 5a shows that $C_{NO_2,L}$ gradually increases with the increase of E_{VOCs} at a fixed E_{NOx} (same as that of TRES). This can be explained as VOC-derived peroxy radicals can play a key role in the conversion of NO to NO_2 through chemistry; in other words, for the fixed E_{NOx}, the increase of $C_{NO_2,L}$ is mainly due to the chemical processing through VOCs. This indicates that all other factors being equal, slightly higher levels of NO_2 will slightly result from more green (i.e. vegetated) areas producing extra E_{VOCs}. However, this neglects the depositional loss of NO_2 to vegetation (Pugh et al., 2012). It is noted that the concentration difference of $C_{NO_2,L}$ between Case HC-HH (η =0.9) and Case HC-LL (η =0.1) gradually increases with the increase of E_{VOCs}, from 23 ppb (at $E_{VOCs} / E_{TRES,VOCs}$ =0.1) to 80 ppb (at $E_{VOCs} / E_{TRES,VOCs}$ =2). This finding indicates that the effect of

the heterogeneity coefficient is more significant for higher E_{VOCs} when keeping E_{NOx} unchanged. Figure 5b shows that $C_{NO_2,L}$ generally increases with the increase of E_{NOx} at a fixed E_{VOCs} (same as that of TRES), with a rapid increase while $E_{NO_x} / E_{TRES,NO_x}$ ranges from 0.1 to 0.5. This is mainly attributed to the fact that the emitted NO_x contributes directly to the increase of $C_{NO_2,L}$. This indicates that adoption of technology controlling NO_x will have a significant effect in reducing NO_2 levels (as would be anticipated). The direct contributions of NO_x emissions to $C_{NO_2,L}$ (assuming no photochemical processes) for cases with different heterogeneity coefficients are indicated by a series of radiating lines in Figure 5b. Any deviation from these radiating lines can be attributed to the contributions from photochemical processes (which convert NO to NO_2). It can be seen from Figure 5b that the chemically induced NO_2 increases rapidly for smaller E_{NOx} and becomes steady for larger E_{NOx}. It is found that the contributions from photochemistry / ozone titration are dominant over those from direct emissions, highlighting the importance of photochemistry in converting NO to NO_2 for the street canyon environment. There is also clear evidence of the reduced impact of the heterogeneity coefficient at lower E_{NOx}. The concentration difference of $C_{NO_2,L}$ between Case HC-HH and Case HC-LL gradually increases with the increase of E_{NOx}, from 13 ppb (at $E_{NO_x} / E_{TRES,NO_x}$ =0.1) to 60 ppb (at $E_{NO_x} / E_{TRES,NO_x}$ =2). Figure 5c illustrates the change of $C_{NO_2,L}$ for TRES-2010 with changing traffic volume only (i.e. E_{VOCs} and E_{NOx} varies proportionally). The pattern of $C_{NO_2,L}$ is a combination of those in Figure 5a and Figure 5b, and a nearly linear relationship is observed. This indicates that controlling the number of vehicles in street canyons with the same fleet composition as the TRES will have an approximately linear effect on the NO_2 levels. This evidence may be used to derive a simple parameterisation scheme for NO_2 with respect to traffic volume. Figure 5d shows the results of $C_{NO_2,L}$ from the year 2005 to 2020. It is observed that $C_{NO_2,L}$ decreases with year. This is mainly attributed to the predicted performance of control technologies applied, which achieve lower E_{VOCs} and E_{NOx}. $C_{NO_2,L}$ begins to attain the air quality standard for hourly NO_2 (for this idealised scenario) from the year 2007 for Case HC-LL (η =0.1), 2009 for

Case HC-L (η =0.3), 2011 for Case BASE (η =0.5), 2014 for Case HC-H (η =0.7) and 2017 for Case HC-HH (η =0.9). $C_{NO_2,L}$ represents the mean concentration of the entire lower box which may still be substantially lower than the highest concentration in the hotspots near the exhaust zone (Zhong et al., 2015).

Figure 6 shows the effect of the heterogeneity coefficient (η) on $\phi_{NO_2,L}$ (%), i.e. the percentage of overestimation for NO_2 in the lower canyon, by the 'one-box' model, compared with the more sophisticated coupled-two-box model approach. Negative values of $\phi_{NO_2,L}$ are observed for all the cases. It is interesting to notice that the magnitude of $\phi_{NO_2,L}$ gradually increases with the increase of heterogeneity coefficient (η), i.e. the range of (-9.54 %, -4.13 %) among all tested emission scenarios for Case HC-LL with η =0.1 (Figure 6a), (-23.94 %, -11.36 %) for Case HC-L with η =0.3 (Figure 6b), (-33.49 %, -17.07 %) for Case BASE with η =0.5 (Figure 6c), (-40.74 %, -21.94 %) for Case HC-H with η =0.7 (Figure 6d) and (-46.73 %, -26.22 %) for Case HC-HH with η =0.9 (Figure 6e). It is also noted that $\phi_{NO_2,L}$ changes nonlinearly with the change of emissions of NO_x and VOCs, which is mainly attributed to nonlinear photochemical reactions. This indicates that for higher VOCs emission rate scenarios (Figure 6), nonlinear photochemistry plays a key role in reducing the percentage of overestimation for NO_2 by the 'one-box' model compared with that for e.g. a passive scalar.

Figure 7 illustrates the transects of $\phi_{NO_2,L}$ (ppb) for Case HC-LL, Case HC-L, Case BASE, Case HC-H and Case HC-HH through the selected lines for analysis in Figure 4f. Figure 7a shows that the magnitude of $\phi_{NO_2,L}$ slightly increases with the increase of E_{VOCs}, i.e. from -4.48 % to -4.59 % for η =0.1, from -11.88 % to -14.26 % for η =0.3, from -18.14% to -24.16 % for η =0.5, from -23.57 % to -33.54 % for η =0.7 and from -28.37 % to -41.88 % for η =0.9. It is noted that the higher the value of heterogeneity coefficient, the larger the magnitude of $\phi_{NO_2,L}$. This indicates that the one box model performance is better for the case with lower heterogeneity coefficients or for

lower VOC emissions (or less "green") areas. Figure 7b shows that the magnitude of $\phi_{NO_2,L}$ generally decreases with the increase of E_{NOx}, except for a slight increase at $E_{NO_x} / E_{TRES,NO_x}$ =0.2 for the cases with η =0.5, η =0.7 and η =0.9. This may be attributed to the complexity of the nonlinear photochemistry in such segregated street canyon environment. Figure 7c also shows that there is no significant change in the $\phi_{NO_2,L}$ when changing both E_{VOCs} and E_{NOx} and that the values of $\phi_{NO_2,L}$ are principally affected by the heterogeneity coefficient (η). This finding is also indicated by Figure 7d, in which the values of $\phi_{NO_2,L}$ do not change significantly over the simulated emissions evolution for the years 2005 to 2020 (the maximum difference is within 5 %) and there is significant contrast between the cases with a difference in heterogeneity coefficient (the contrast is around 10 % for the interval of η =0.2).

3.2 Effect of the exchange velocity

Figure 8 illustrates the effect of the exchange velocity ($w_{t,0}$) on $C_{NO_2,L}$ (ppb), i.e. the concentration in the lower box, for (a) Case EX-LL ($w_{t,0}$ =0.012 m s^{-1}), (b) Case EX-L ($w_{t,0}$ =0.016 m s^{-1}), (c) Case BASE ($w_{t,0}$ =0.02 m s^{-1}), (d) Case EX-H ($w_{t,0}$ =0.024 m s^{-1}) and (e) Case EX-HH ($w_{t,0}$ =0.028 m s^{-1}). $w_{t,0}$ has a direct effect on the pollutant concentration in the one-box homogenous system (also representing the whole canyon averaged pollutant concentration in the two-box system) and plays an important role in determining the lower canyon pollutant concentration in the two box system for given scenario conditions (Section 2). $w_{t,0}$ can vary with the external wind turbulence above the street canyon, the street canyon geometry and the stability of the atmosphere. It is observed that $C_{NO_2,L}$ is significantly influenced by $w_{t,0}$. For Case EX-LL, levels of $C_{NO_2,L}$ are extremely high (the maximum value could be up to 350 ppb). This corresponds to the lowest $w_{t,0}$ adopted in Case EX-LL, which gives the worst (lowest) exchange between the lower and upper box (indicated by a lower value of $w_{t,L}$ in Figure 3). Therefore, pollutants are not efficiently carried from the lower box to the overlying canopy layer. It is interesting to notice that the solid red curve

(representing the UK air quality standard for hourly NO_2) shifts from the region with lower emissions to that with higher emissions as $w_{t,0}$ increases. This means that even low emissions under the worst dispersion conditions can result in very poor air quality inside street canyons. It is also observed that trajectory 2005-2020 falls entirely into the region representing a breach of the UK air quality standard for hourly NO_2 for Case EX-LL with the lowest $w_{t,0}$, for this idealised scenario. With the increase of the exchange velocity, the solid red curve moves from the year 2020 towards the year 2005. It is also noted that TRES is in the region breaching the UK air quality standard for hourly NO_2 for Case EX-LL, Case EX-L and Case BASE, but is within the air quality limit for Case EX-H and Case EX-HH. The detailed results along the selected lines for analysis, shown as Figure 4f, are presented below.

Figure 9 shows the transects of $C_{NO_2,L}$ (ppb) for Case EX -LL, Case EX-L, Case BASE, Case EX-H and Case EX-HH through the selected lines for analysis as shown in Figure 4f. It is also observed that $C_{NO_2,L}$ increases with the increase in E_{VOCs} and E_{NOx}, shown as Figure 9a-c. This indicates that the control of either E_{VOCs} or E_{NOx} is effective to reduce the NO_2 levels, in the former case via repartitioning of NO_x. It is also interesting to notice that there is less change of $C_{NO_2,L}$ where E_{VOCs} is lower. The minimum and maximum differences of $C_{NO_2,L}$ between Case EX-LL with $w_{t,0}$ =0.012 m s^{-1} and Case EX -HH with $w_{t,0}$ =0.028 m s^{-1} are 44 ppb and 201 ppb for Figure 9a, 15 ppb and 136 ppb for Figure 9b, and 17 ppb and 228 ppb for Figure 9c. This indicates the importance of controlling ventilation conditions of street canyons especially for highly polluted scenarios. The direct contributions of NO_x emissions to $C_{NO_2,L}$ for cases with different exchange velocities are represented by a series of radiating lines in Figure 9b, which indicates that photochemical processes (primarily ozone titration) contribute more to NO_2 than direct emissions. It is also found that the chemically induced NO_2 increases rapidly for smaller E_{NOx} and becomes negligible for larger E_{NOx}, due to the limited ozone supply Figure 9d shows that $C_{NO_2,L}$ decreases significantly with year due to the (predicted) influence of vehicle control technologies upon both E_{VOCs} and E_{NOx}. This indicates

that the air quality will be improved in future years. However, for the worst ventilation condition (e.g. Case EX-LL), $C_{NO_2,L}$ is still in the breach of the UK air quality standard for hourly NO_2 over the year 2005 to 2020. This indicates that control of air ventilation together with control of vehicle emissions is important in improving air quality within street canyons. Air ventilation is strongly influenced by the urban street design and deep street canyons could lead to poor ventilation.

Figure 10 shows the effect of the exchange velocity ($w_{t,0}$) on $\phi_{NO_2,L}$ (%), i.e. the percentage of overestimation for NO_2 in the lower canyon by the 'one-box' model, compared with the two-box system. It is found that $\phi_{NO_2,L}$ decreases slightly with increasing exchange velocity ($w_{t,0}$), i.e. the range of (-37.49 %, -17.64 %) among all tested emission scenarios for Case EX-LL (-35.26 %, -17.22 %) for Case EX-L, (-33.49 %, -17.07 %) for Case BASE, (-31.89 %, -17.02 %) for Case EX-H and (-30.52 %, -17.01 %) for Case EX-HH. As η =0.5 is adopted for all cases in Figure 10, the nonlinear patterns reflect the characteristics of scenarios with a single heterogeneity coefficient. This indicates that there is a systematic underestimation of NO_2 concentrations by the 'one-box' model and this underestimation changes significantly with the heterogeneity coefficient (Figure 4), to a much greater extent than the change with the exchange velocity (Figure 10).

Figure 11 illustrates the transects of $\phi_{NO_2,L}$ (ppb) for Case EX -LL, Case EX-L, Case BASE, Case EX-H and Case EX-HH through the selected lines for analysis in Figure 4f. Figure 11a shows that $\phi_{NO_2,L}$ decreases modestly with the increase of E_{VOCs}, i.e. from -21.15 % to -26.86 % for Case EX-LL, from -19.26 % to -25.37 % for Case EX-L, from -18.14 % to -24.16 % for Case BASE, from -17.48 % to -23.16 % for Case EX-H and from -17.15 % to -22.36 % for Case EX-HH. Figure 11b shows that $\phi_{NO_2,L}$ generally increases with the increase of E_{NOx}, except a slight decrease at $E_{NO_x} / E_{TRES,NO_x}$ =0.2. Figure 11c shows that there is no significant difference between the cases with different exchange velocities (within 5 %) while both E_{VOCs} and E_{NOx} are below half of those

for TRES. For the emission predictions corresponding to the years 2005 to 2020 shown as Figure 11d, there is also no significant change of $\phi_{NO_2,L}$ (within 5 % difference).

3.3 Effect of the box height ratio

Figure 12 illustrates the effect of the box height ratio (α) on $C_{NO_2,L}$ (ppb), i.e. the concentration in the lower box, for Case HB-LL (α =0.1), (b) Case HB-L (α =0.3), (c) Case BASE (α =0.5), (d) Case HB-H (α =0.7), and (e) Case HB-HH (α =0.9). The value of α can vary with the flow structure in a street canyon, which may be significantly influenced by the building geometry. A high-level circulation induced for example by a pitched building roof will give a smaller relative size of the upper vortex (Louka et al., 2000), corresponding to a higher value of α (possibly equivalent to 0.9). Large eddy simulations of street canyons by Li et al. (2012) suggested that the street bottom heating may have a strong impact on the flow pattern within a deep street canyon (AR=2), i.e. the value of α can about 0.44 under the neutral condition, about 0.46 under weak heating and about 0.9 under strong heating. There is clear evidence in Figure 12 that $C_{NO_2,L}$ is significantly affected by the box height ratio. Extremely high levels of $C_{NO_2,L}$ are observed for smaller box height ratios, e.g. with a maximum value of about 520 ppb for Case HB-LL with α =0.1. This small box height ratio represents the case that pollutants are essentially trapped in a low volume part of the street canyon under poor ventilation conditions. This is similar to the secondary smaller eddies near the street corner, where levels of pollutants can be extremely high. The exchange velocity between lower and upper boxes (indicated by a lower value of $w_{t,L}$ in Figure 3) is the lowest for Case HB-LL. It is observed that almost all of the scenarios (including trajectory 2005-2020) in Case HB-LL are expected to breach the UK air quality standard for hourly NO_2, for this idealised scenario, except for scenarios with extremely low emissions, shown as Figure 12a. As the box height ratio increases, the solid red curve in Figure 12 shifts towards scenarios with higher emissions across the trajectory for predicted emissions 2005-2020. For Case HB-H and Case HB-HH, the TRES falls into the region below the UK air quality standard for hourly NO_2. The box

500 height ratio is mainly determined by the flow structure in the street canyon. Therefore,
501 understanding the flow characteristics in a street canyon is of vital importance; numerical modelling
502 approaches can provide predictions of flow patterns at high spatial and temporal resolution within
503 street canyons. The detailed results along the selected lines for analysis, shown as Figure 4f, are
504 presented below.

505 Figure 13 shows the transects of $C_{NO_2,L}$ (ppb) for Case HB-LL, Case HB-L, Case BASE, Case HB-
506 H and Case HB-HH through the selected lines for analysis in Figure 4f. It can be seen that there is
507 an increase of $C_{NO_2,L}$ with the increase of E_{VOCs} and E_{NOx}. This increasing tendency is extremely
508 significant for Case HB-LL with the lowest box height ratio (α =0.1), i.e. 207 ppb difference for
509 Figure 13a, 302 ppb difference for Figure 13b and 461 ppb difference for Figure 13c. For other box
510 height ratios in Figure 13a-c, the concentration difference is around 100 ppb, much lower than that
511 for Case HB-LL. The direct contributions of NO_x emissions to $C_{NO_2,L}$ for cases with different box
512 height ratios are represented by the series of radiating lines in Figure 13b, which also indicates the
513 importance of photochemistry in converting NO to NO_2, rather than the contribution from direct
514 emissions of NO_2. A rapid increase of the chemically induced NO_2 for smaller E_{NOx} is also observed.
515 Figure 13d shows that there is a decrease of $C_{NO_2,L}$ with years for the corresponding predicted
516 emissions. However, the air quality is still worse for Case HB-LL and Case HB-L, i.e. about 4
517 times and 2 times of the UK air quality standard for hourly NO_2 for the year 2005, for this idealised
518 scenario.

519 Figure 14 shows the effect of the box height ratio (α) on $\phi_{NO_2,L}$ (%), i.e. the percentage of
520 overestimation for NO_2 in the lower canyon, by the 'one-box' model. There are significant changes
521 of $\phi_{NO_2,L}$ with the changes of the box height ratio, i.e. (-82.22 %, -57.37 %) for Case HB-LL with
522 α=0.1, (-54.15 %, -30.26 %) for Case HB-L with α=0.3, (-33.49 %, -17.07 %) for Case BASE
523 with α=0.5, (-17.71 %, -8.63 %) for Case HB-H with α=0.7 and (-5.27 %, -2.59 %) for Case HB-
524 HH with α=0.9. This indicates that for a higher box height ratio, the 'one-box' model more

accurately predicts NO_2 concentrations, as referenced to the coupled-two-box simulation. It is also noted that $\phi_{NO_2,L}$ is less sensitive to emissions of NO_x and VOCs when the box height ratio is higher. For the extremely high box height ratios, the upper box plays a similar role as the shear layer, where active exchange takes place. In such a situation, the two-box model can approximate to the one-box model.

Figure 15 illustrates the transects of $\phi_{NO_2,L}$ (ppb) for Case HB-LL, Case HB-L, Case BASE, Case HB-H and Case HB-HH through the selected lines for analysis in Figure 4f. Figure 15a shows that the magnitude of $\phi_{NO_2,L}$ slightly increases with the increase of E_{VOCs}, i.e. from -64.94 % to -72.29 % for α=0.1, from -33.18 % to -41.62 % for α=0.3, from -18.14% to -24.16 % for α=0.5, from -8.98 % to -12.37 % for α=0.7 and from -2.65 % to -3.65 % for α=0.9. This indicates that the difference in $\phi_{NO_2,L}$ decreases with an increase in the box height ratio, and the one box model performs better for the cases with a higher box height ratio. This finding is also indicated by Figure 15b, but the magnitude of $\phi_{NO_2,L}$ slightly decreases with the increase of E_{NOx}, especially for $E_{NO_x} / E_{TRES,NO_x}$ up to 0.5. Figure 15c also shows that there is no significant change in $\phi_{NO_2,L}$ when changing both E_{VOCs} and E_{NOx} and that $\phi_{NO_2,L}$ is mainly influenced by the box height ratio (α). Figure 15d shows that $\phi_{NO_2,L}$ does not change significantly for the predicted emissions changes over the years 2005 to 2020, but significant contrasts are found for the cases with different box height ratios.

4 Conclusions

The bulk levels of air pollution within a street canyon, focusing on the lower heights where pedestrian / human exposure takes place, are investigated using a coupled-two-box model approach, which enables a wide range of emission scenarios to be considered in a computationally efficient manner, whilst providing greater realism than a single, well-mixed box approach. The performance of the one-box model approach (assuming the whole street canyon as a well-mixed box) was also examined compared with the bulk concentrations in the lower canyon of the two-box model. Core

549 important parameters (i.e. heterogeneity coefficient, exchange velocity and box height ratio) related
550 to the two-box model approach were investigated. The two-box model results identify the emission
551 regimes and the meteorological conditions under which NO_2 in the lower canyon (street level) is in
552 breach of air quality standards. Higher NO_2 levels were observed for the cases with higher
553 heterogeneity coefficients (the two boxes are more segregated), or with lower exchange velocities
554 (worse ventilation conditions) or with smaller box height ratios (reduced dilution possibly due to
555 secondary smaller eddies in the lower canyon). The one-box model was found to systematically
556 underestimate NO_2 levels compared with those in the lower box of the two-box model for all the
557 test scenarios. This underestimation generally tends to worsen for higher heterogeneity coefficients,
558 lower exchange velocities, or smaller box height ratios. This study highlights the limitation of the
559 assumption of homogeneity in single box models for street canyon simulation, and the inherent
560 uncertainties that must be borne in mind to appropriately interpret such model output (in particular,
561 that a single-box treatment will systematically underestimate NO_2 as experienced at street level).
562 The assumption of 'exchange velocity' adopted in the two-box model approach only represents the
563 overall integrated effect of the dynamical flow between simplified street canyon boxes, failing to
564 capture the structure of flow and pollutant distribution inside street canyons. The box model
565 approach only provides mean concentrations within the boxes and assumes an instant and complete
566 mixing, thus artificially augmenting chemical reaction rates within the boxes (i.e. generally
567 enhancing the NO to NO_2 conversion rate such that NO_2 would be overestimated) (Zhong et al.
568 (2015); Bright et al. (2013)). In addition, the two-box model approach (vertically segregated) is
569 restricted to represent two vortices within a street canyon. For even taller canyons, more vortices
570 may be formed. Future studies should adopt more photochemical boxes and use finite exchange
571 velocities to allow an incomplete mixing across boxes (thus to be closer to the real conditions), and
572 extend the range of scenarios to encompass the range encountered in reality. Reactive pollutant
573 abundance could be obtained by running the two-box model if a set of parameters are provided for
574 real urban areas as the model inputs (e.g. heterogeneity coefficient, exchange velocity, box height

ratio and emissions) although these three parameters are might be uncontrollable and site- and flow-dependent. For an application in future, it is needed to map the 'controllable pre-defined building geometry parameters' and meteorological conditions to the three box-model parameters we proposed in this study using available knowledge, datasets (e.g. wind tunnel experiments), and/or modelling tools (e.g. CFD). In addition, a standard procedure for setting the parameters used in the two-box model should be developed. A multi-box air quality model for a street canyon network may then be developed for practical applications.

Acknowledgements

The authors would like to thank Dr Vivien Bright for provision of the reduced chemical scheme (RCS). The authors appreciate the University of Birmingham's BlueBEAR HPC service (http://www.bear.bham.ac.uk) for providing the computational resource. JZ thanks the University of Birmingham for the award of a Li Siguang Scholarship, which is offered in partnership with the China Scholarship Council (CSC).

Appendix A: RCS mechanism

Table A1 All reactions and rate constants included in the RCS mechanism (adopted from Bright (2013)). The units of rate constants are s^{-1} for first order reactions and ppb s^{-1} for second order reactions. The pressure is set to 10132.5 Pa and the temperature is set to 293 K.

	Reactants				Products			Rate constant
1	O_3			→	OH	+	OH	3.40E-6
2	NO	+	O_3	→	NO_2			4.01E-4
3	NO	+	NO	→	NO_2	+	NO_2	2.63E-9
4	NO	+	NO_3	→	NO_2	+	NO_2	6.56E-1
5	OH	+	O_3	→	HO_2			1.72E-3
6	OH	+	H_2	→	HO_2			1.49E-4
7	OH	+	CO	→	HO_2			5.06E-3
8	H_2O_2	+	OH	→	HO_2			4.21E-2
9	HO_2	+	O_3	→	OH			4.86E-5
10	OH	+	HO_2	→				2.82E+0
11	HO_2	+	HO_2	→	H_2O_2			8.74E-2
12	HO_2	+	HO_2	→	H_2O_2			6.92E-2
13	OH	+	NO	→	HONO			2.54E-1
14	OH	+	NO_2	→	HNO_3			3.08E-1
15	OH	+	NO_3	→	HO_2	+	NO_2	5.01E-1
16	HO2	+	NO	→	OH	+	NO_2	2.27E-1
17	HO2	+	NO_2	→	HO_2 NO_2			3.59E-2
18	HO_2NO2			→	HO2	+	NO_2	3.74E-2
19	HO_2NO_2	+	OH	→	NO_2			1.20E-1
20	HONO	+	OH	→	NO_2			2.58E-2
21	HNO_3	+	OH	→	NO_3			4.08E-3
22	H_2O_2			→	OH	+	OH	7.11E-6
23	NO_2			→	NO	+	O_3	9.20E-3
24	NO_3			→	NO			2.34E-2
25	NO_3			→	NO_2	+	O_3	1.83E-1
26	HONO			→	OH	+	NO	2.02E-3

27	HNO_3			→	OH	+	NO_2					6.30E-7
28	CH_4	+	OH	→	CH_3O_2							1.39E-4
29	C_2H_4	+	OH	→	$HOCH_2CH_2O_2$							2.00E-1
30	C_3H_6	+	OH	→	RN_9O_2							7.19E-1
31	C_2H_4	+	O_3	→	HCHO	+	CO	+	HO_2	+	OH	4.46E-9
32	C_2H_4	+	O_3	→	HCHO	+	HCOOH					2.99E-8
33	C_3H_6	+	O_3	→	HCHO	+	CH_3O_2	+	CO	+	OH	8.18E-8
34	C_3H_6	+	O_3	→	HCHO	+	CH_3CO_2H					1.45E-7
35	C_5H_8	+	OH	→	RU14O2							2.58E+0
36	C_5H_8	+	O_3	→	UCARB10	+	CO	+	HO_2	+	OH	7.76E-8
37	C_5H_8	+	O_3	→	UCARB10	+	HCOOH					2.10E-7
38	HCHO			→	CO	+	HO_2	+	HO_2			3.05E-5
39	HCHO			→	H_2	+	CO					4.61E-5
40	CH_3CHO			→	CH_3O_2	+	HO_2	+	CO			5.07E-6
41	HCHO	+	OH	→	HO_2	+	CO					2.35E-1
42	CH_3CHO	+	OH	→	CH_3CO_3							4.02E-1
43	CH_3OH	+	OH	→	HO_2	+	HCHO					2.31E-2
44	C_2H_5OH	+	OH	→	CH_3CHO	+	HO_2					7.24E-2
45	C_2H_5OH	+	OH	→	$HOCH_2CH_2O_2$							9.23E-3
46	HCOOH	+	OH	→	HO_2							1.13E-2
47	CH_3CO_2H	+	OH	→	CH_3O_2							2.00E-2
48	CH_3O_2	+	NO	→	HCHO	+	HO_2	+	NO_2			1.95E-1
49	$HOCH_2CH_2O_2$	+	NO	→	HCHO	+	HCHO	+	HO_2	+	NO_2	1.68E-1
50	$HOCH_2CH_2O_2$	+	NO	→	$HOCH_2CHO$	+	HO_2	+	NO_2			4.84E-2
51	RN_9O_2	+	NO	→	CH_3CHO	+	HCHO	+	HO_2	+	NO_2	2.13E-1
52	CH_3CO_3	+	NO	→	CH_3O_2	+	NO_2					5.10E-1
53	$HOCH_2CO_3$	+	NO	→	HO_2	+	HCHO	+	NO_2			5.10E-1
54	$RU14O_2$	+	NO	→	UCARB12	+	HO_2	+	NO_2			4.93E-2
55	$RU14O_2$	+	NO	→	UCARB10	+	HCHO	+	HO_2	+	NO_2	1.46E-1
56	$RU12O_2$	+	NO	→	CH3CO3	+	$HOCH_2CHO$	+	NO_2			1.52E-1
57	$RU12O_2$	+	NO	→	CARB7	+	CO	+	HO_2	+	NO_2	6.52E-2
58	$RU10O_2$	+	NO	→	CH3CO3	+	$HOCH_2CHO$	+	NO_2			1.09E-1

59	$RU10O_2$	+	NO	→	CARB6	+	HCHO	+	HO_2	+	NO_2	6.52E-2
60	$RU10O_2$	+	NO	→	CARB7	+	HCHO	+	HO_2	+	NO_2	4.35E-2
61	CH_3O_2	+	NO	→	CH_3NO_3							1.95E-4
62	$HOCH_2CH_2O_2$	+	NO	→	$HOC_2H_4NO_3$							1.09E-3
63	RN_9O_2	+	NO	→	$RN9NO_3$							4.56E-3
64	$RU14O_2$	+	NO	→	$RU14NO_3$							2.17E-2
65	CH_3O_2	+	HO_2	→	CH_3OOH							1.52E-1
66	$HOCH_2CH_2O_2$	+	HO_2	→	HOC_2H_4OOH							3.62E-1
67	$RN9O_2$	+	HO_2	→	RN9OOH							3.20E-1
68	CH_3CO_3	+	HO_2	→	CH_3CO_3H							3.75E-1
69	$HOCH_2CO_3$	+	HO_2	→	$HOCH_2CO_3H$							3.75E-1
70	$RU14O_2$	+	HO_2	→	RU14OOH							4.74E-1
71	$RU12O_2$	+	HO_2	→	RU12OOH							4.35E-1
72	$RU10O_2$	+	HO_2	→	RU10OOH							3.85E-1
73	CH_3O_2			→	HCHO	+	HO_2					6.22E-3*
74	CH_3O_2			→	HCHO							6.32E-3*
75	CH_3O_2			→	CH_3OH							6.32E-3*
76	$HOCH_2CH_2O_2$			→	$HOCH_2CHO$	+	HO_2					1.12E-2*
77	$RN9O_2$			→	CH_3CHO	+	HCHO	+	HO_2			2.20E-2*
78	CH_3CO_3			→	CH_3O_2							2.50E-1*
79	$HOCH_2CO_3$			→	HCHO	+	HO_2					2.50E-1*
80	$RU14O_2$			→	UCARB12	+	HO_2					1.08E-2*
81	$RU14O_2$			→	UCARB10	+	HCHO	+	HO_2			3.20E-2*
82	$RU12O_2$			→	CH_3CO_3	+	HOCH2CHO					3.51E-2*
83	$RU12O_2$			→	CARB7	+	HOCH2CHO	+	HO_2			1.50E-2*
84	$RU10O_2$			→	CH_3CO_3	+	$HOCH_2CHO$					2.50E-2*
85	$RU10O_2$			→	CARB6	+	HCHO	+	HO_2			1.50E-2*
86	$RU10O_2$			→	CARB7	+	HCHO	+	HO_2			1.00E-2*
87	CARB7			→	CH3CO3	+	HCHO	+	HO_2			3.36E-6
88	$HOCH_2CHO$			→	HCHO	+	CO	+	HO_2	+	HO_2	1.77E-5
89	UCARB10			→	CH_3CO_3	+	HCHO	+	HO_2			1.62E-5
90	CARB6			→	CH_3CO_3	+	CO	+	HO2			1.26E-4

91	UCARB12			→	CH_3CO_3	+	HOCH2CHO	+	CO	+	HO2	1.62E-5
92	CARB7	+	OH	→	CARB6	+	HO_2					7.51E-2
93	UCARB10	+	OH	→	$RU10O_2$							6.26E-1
94	UCARB10	+	O_3	→	HCHO	+	CH_3CO_3	+	CO	+	OH	4.21E-8
95	UCARB10	+	O_3	→	HCHO	+	CARB6	+	H_2O_2			2.93E-8
96	$HOCH_2CHO$	+	OH	→	$HOCH_2CO_3$							2.50E-1
97	CARB6	+	OH	→	CH_3CO_3	+	CO					4.31E-1
98	UCARB12	+	OH	→	$RU12O_2$							1.13E-0
99	UCARB12	+	O_3	→	$HOCH_2CHO$	+	CH_3CO_3	+	CO	+	OH	5.35E-7
100	UCARB12	+	O_3	→	$HOCH_2CHO$	+	CARB6	+	H_2O_2			6.61E-8
101	CH_3NO_3			→	HCHO	+	HO_2	+	NO_2			8.96E-7
102	CH_3NO_3	+	OH	→	HCHO	+	NO_2					9.33E-3
103	$HOC_2H_4NO_3$	+	OH	→	$HOCH_2CHO$	+	NO_2					2.73E-2
104	$RN9NO_3$	+	OH	→	CARB7	+	NO_2					3.28E-2
105	$RU14NO_3$	+	OH	→	UCARB12	+	NO_2					1.39E+0
106	CH_3OOH			→	HCHO	+	HO_2	+	OH			5.44E-6
107	CH_3CO_3H			→	CH_3O_2	+	OH					5.44E-6
108	$HOCH_2CO_3H$			→	HCHO	+	HO_2	+	OH			5.44E-6
109	RU14OOH			→	UCARB12	+	HO_2	+	OH			1.37E-6
110	RU14OOH			→	UCARB10	+	HCHO	+	HO_2	+	OH	4.07E-6
111	RU12OOH			→	CARB6	+	HOCH2CHO	+	HO_2	+	OH	5.44E-6
112	RU10OOH			→	CH_3CO_3	+	HOCH2CHO	+	OH			5.44E-6
113	HOC_2H_4OOH			→	HCHO	+	HCHO	+	HO_2	+	OH	5.44E-6
114	RN9OOH			→	CH_3CHO	+	HCHO	+	HO_2	+	OH	5.44E-6
115	CH_3OOH	+	OH	→	CH_3O_2							9.10E-1
116	CH_3OOH	+	OH	→	HCHO	+	OH					4.79E-1
117	CH_3CO_3H	+	OH	→	CH_3CO_3							9.27E-2
118	$HOCH_2CO_3H$	+	OH	→	$HOCH_2CO_3$							1.55E-1
119	RU14OOH	+	OH	→	UCARB12	+	OH					1.88E+0
120	RU12OOH	+	OH	→	$RU12O_2$							7.51E-1
121	RU10OOH	+	OH	→	$RU10O_2$							7.51E-1
122	HOC_2H_4OOH	+	OH	→	$HOCH_2CHO$	+	OH					5.34E-1

123	RN9OOH	+	OH	→	CARB7	+	OH			6.26E-1
124	CH_3CO_3	+	NO_2	→	PAN					2.68E-1
125	PAN			→	CH_3CO_3	+	NO_2			1.51E-4
126	$HOCH_2CO_3$	+	NO_2	→	PHAN					2.68E-1
127	PHAN			→	$HOCH_2CO_3$	+	NO_2			1.51E-4
128	PAN	+	OH	→	HCHO	+	CO	+	NO_2	2.59E-3
129	PHAN	+	OH	→	HCHO	+	CO	+	NO_2	2.81E-2
130	$RU12O_2$	+	NO_2	→	RU12PAN					1.63E-2
131	RU12PAN			→	$RU12O_2$	+	NO_2			1.51E-4
132	$RU10O_2$	+	NO_2	→	MPAN					1.10E-2
133	MPAN			→	$RU10O_2$	+	NO_2			1.51E-4
134	MPAN	+	OH	→	CARB7	+	CO	+	NO_2	9.02E-2
135	RU12PAN	+	OH	→	UCARB10	+	NO_2			6.31E-1
136	NO_2	+	O_3	→	NO_3					7.65E-7

Note: * means peroxy radical summation, which is applied to the RO_2 permutation reactions.

$[RO_2] = [CH_3O_2] + [HOCH_2CH_2O_2] + [RN9O_2] + [CH_3CO_3] + [HOCH_2CO_3] + [RU14O_2] + [RU12O_2] + [RU10O_2]$

602

603

604

605

606

607

608

609

610

611

612 **Table 1 Overview of the model scenarios**

Case	Heterogeneity coefficient (η)	Exchange velocity $w_{t,0}$ (m s^{-1})	Box height ratio (α)
BASE	0.5	0.02	0.5
HC-LL	0.1	0.02	0.5
HC-L	0.3	0.02	0.5
HC-H	0.7	0.02	0.5
HC-HH	0.9	0.02	0.5
EX-LL	0.5	0.012	0.5
EX-L	0.5	0.016	0.5
EX-H	0.5	0.024	0.5
EX-HH	0.5	0.028	0.5
BH-LL	0.5	0.02	0.1
BH-L	0.5	0.02	0.3
BH-H	0.5	0.02	0.7
BH-H	0.5	0.02	0.9

Note: 'BASE' is the base case. 'HC' denotes the heterogeneity coefficient; 'EX' denotes the exchange velocity; 'BH' denotes the box height ratio. 'LL', 'L', 'H' and 'HH' represent a even lower, lower, higher and even higher value than the corresponding component in the case BASE, respectively.

613

614

615

616

617

618

619

620

621

622 **(a)** **(b)**

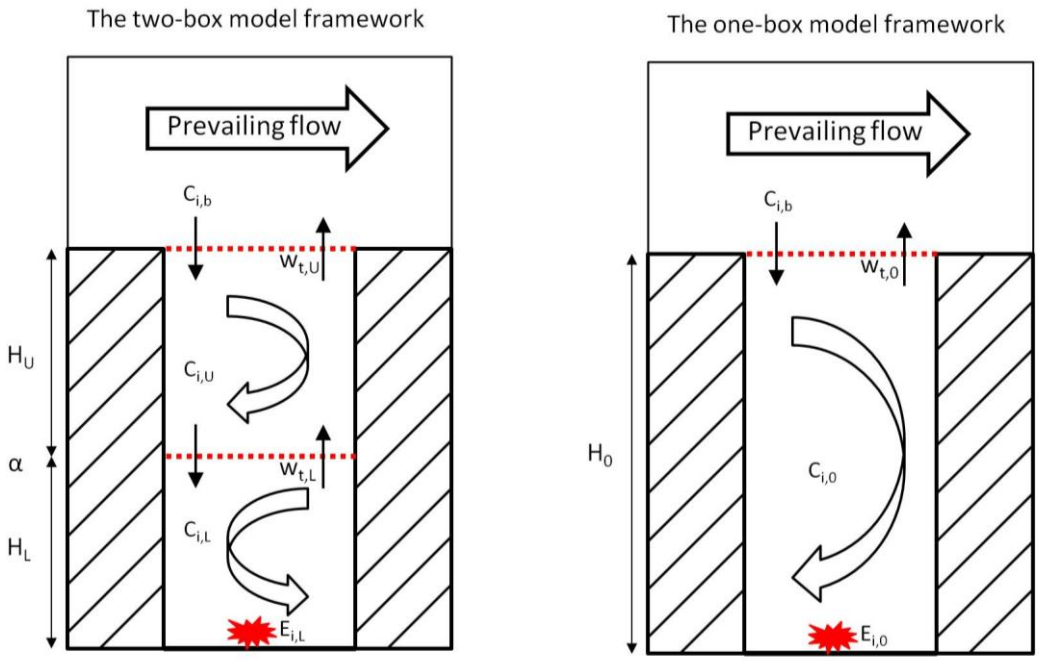

623

624 **Figure 1 Framework of the coupled two-box and one-box models (see text for details).**

625

626

627

628

629

630

631

632

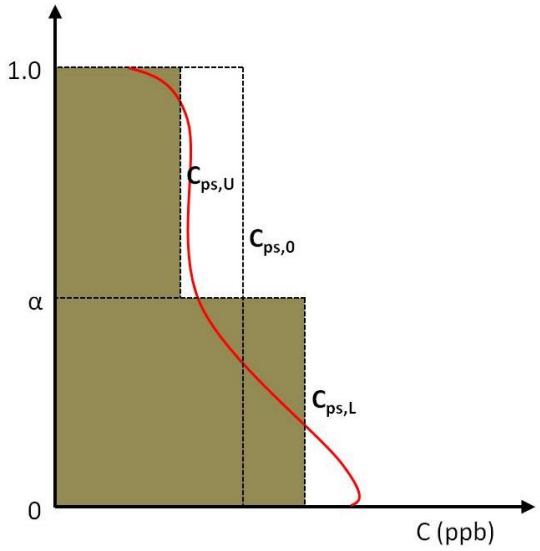

633

634

635 **Figure 2 Schematic diagram of the vertical concentration profile and bulk concentrations in the lower and upper**

636 **boxes, and in the whole street canyon of passive scalar.**

637

638

639

640

641

642

643

644

645

646

647

648

649

650 **(a)** **(b)** **(c)**

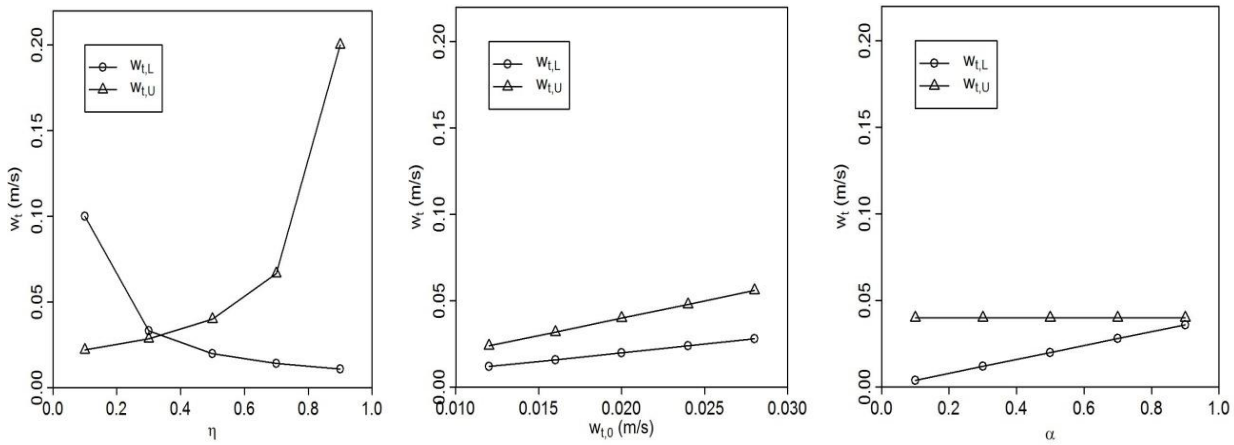

651

652 **Figure 3 The relationship between exchange velocities for the two-box model against (a)** η **when** $\alpha = 0.5$, **(b)**

653 $w_{t,0}$ **when** $\alpha = 0.5$ **and** $\eta = 0.5$, **and (c)** α **when** $\eta = 0.5$ **and** $w_{t,0} = 0.02$ **(m s^{-1}). See Equations 13-14.**

654

655

656

657

658

659

660

661

662

663

664

665

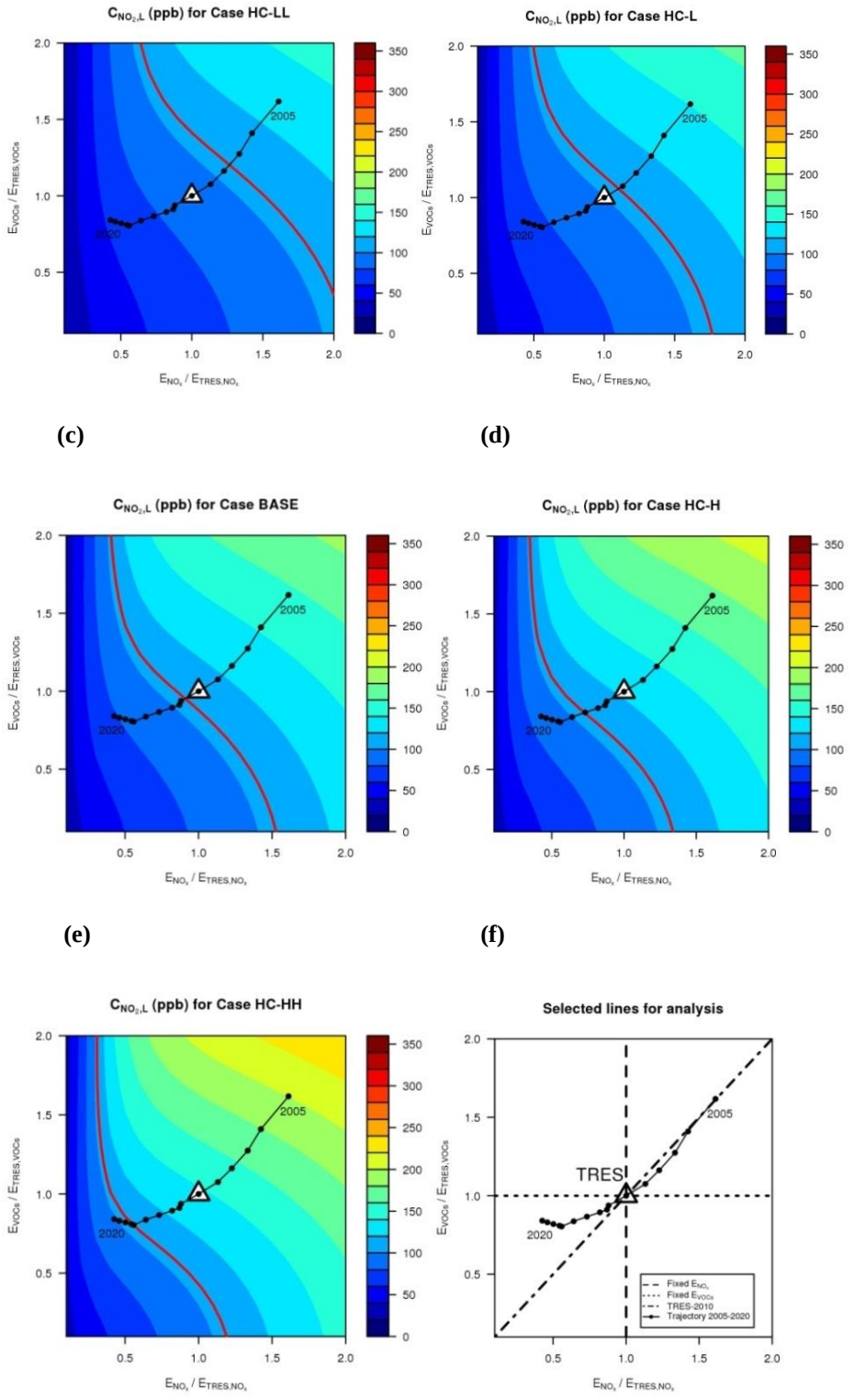

Figure 4 $C_{NO_2,L}$ **(ppb), i.e. the concentration in the lower box derived from the "two-box" model, in the (a) Case HC-LL (**η**=0.1), (b) Case HC-L (**η**=0.3), (c) Case BASE (**η**=0.5), (d) Case HC-H (**η**=0.7), (e) Case HC-HH (**η**=0.9) and (f) Selected lines for analysis.** E_{VOCs} **and** E_{NOx} **are normalised by those of the Typical Real-world Emission Scenario (TRES, represented by△), for the year of 2010. Trajectory 2005-2020 represents the emission scenarios for 2005 to 2020, assuming constant traffic volume and speed. The solid red curves denote the UK air quality standard for hourly NO_2 (105 ppb).**

679 **(a)** **(b)**

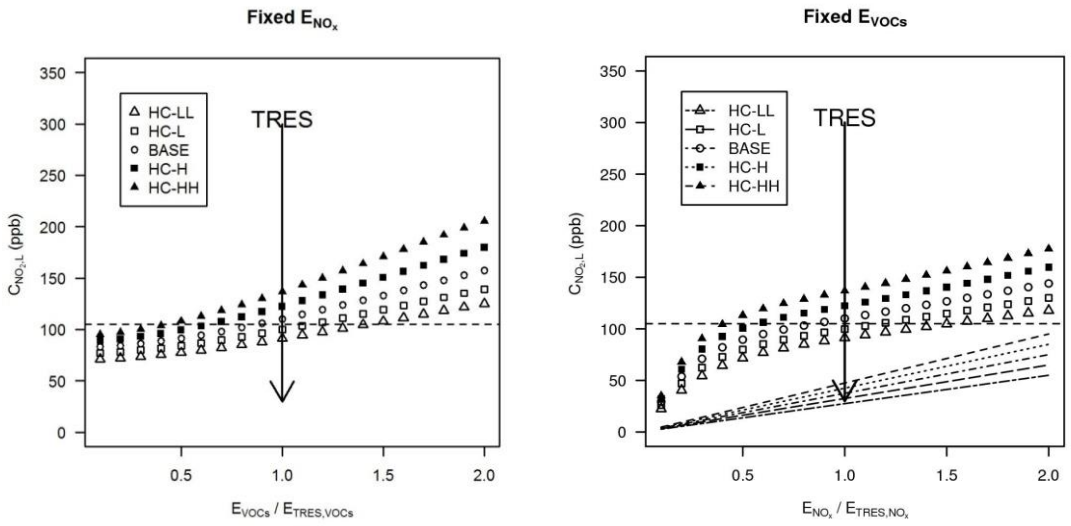

680

681 **(c)** **(d)**

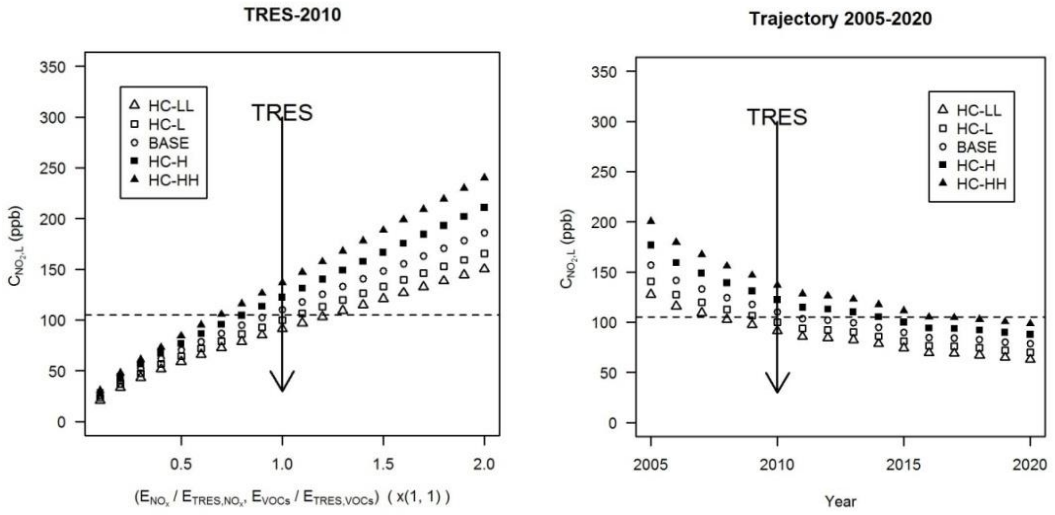

682

683 **Figure 5 $C_{NO_2,L}$ (ppb), i.e. the concentration in the lower box derived from the "two-box" model, for (a) "Fixed**
684 **E_{NOx}" at a fixed NO_x emissions of TRES, (b) "Fixed E_{VOCs}" at a fixed VOCs emissions of TRES (The direct**
685 **contributions of NO_x emissions to $C_{NO_2,L}$ are indicated by a series of radiating lines, running from highest to**
686 **lowest for the cases from HC-HH to HC-LL.), (c) "TRES-2010" varying the total traffic volume only and (d)**
687 **"Trajectory 2005-2020" assuming constant traffic volume and speed varying η. E_{VOCs} and E_{NOx} are normalised**
688 **by those of the Typical Real-world Emission Scenario (TRES, represented by△), for the year of 2010. The**
689 **dashed line indicates the UK air quality standard for hourly NO_2 (105 ppb).**

690

691

692

693

694

695

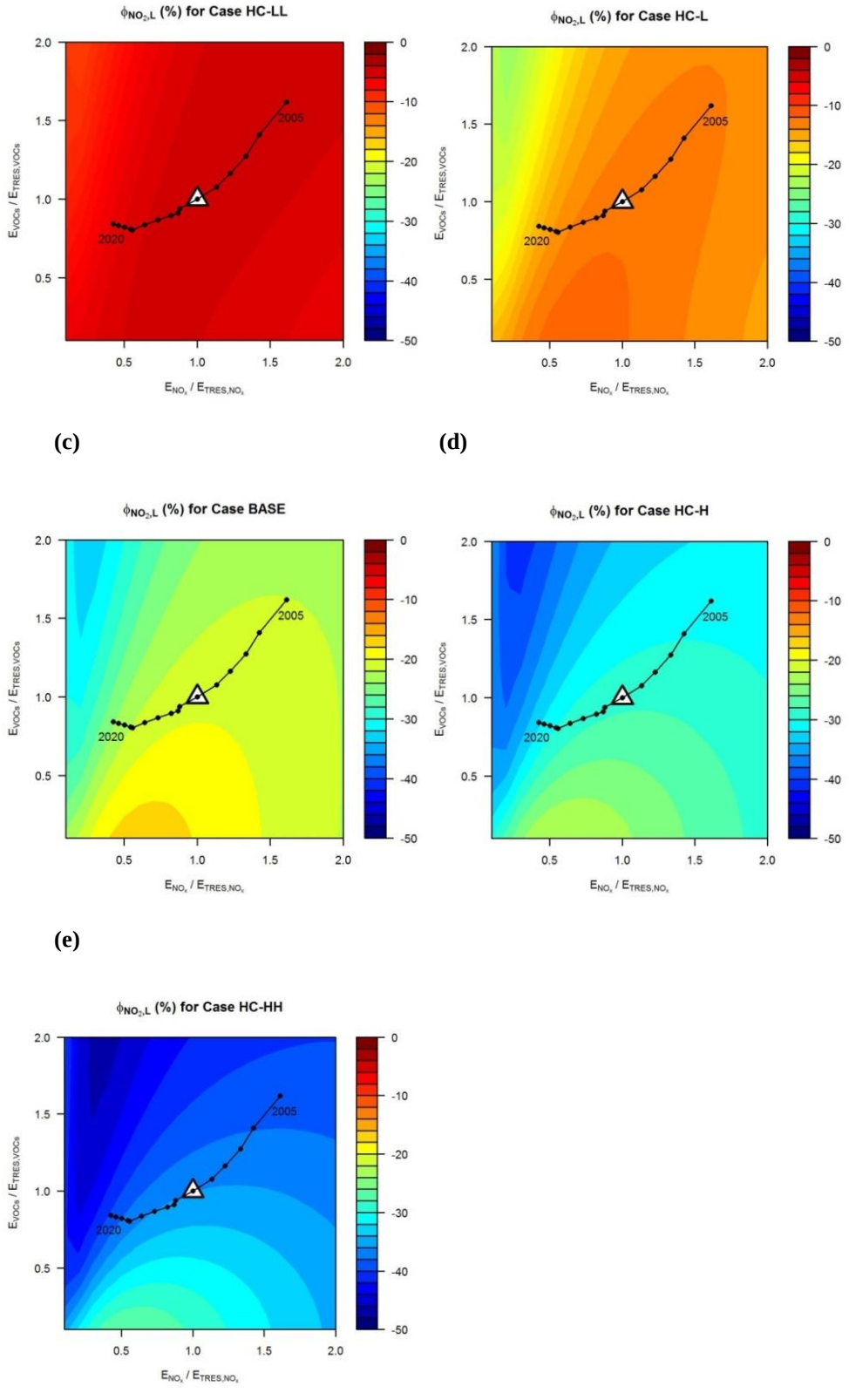

Figure 6 $\phi_{NO_2,L}$ (%), i.e. the percentage of overestimation for NO_2 in the lower canyon by the 'one-box' model compared with that by the "two-box" model, in the (a) Case HC-LL (η =0.1), (b) Case HC-L (η =0.3), (c) Case BASE (η =0.5), (d) Case HC-H (η =0.7), (e) Case HC-HH (η =0.9). E_{VOCs} and E_{NOx} are normalised by those of the Typical Real-world Emission Scenario (TRES, represented by△), for the year of 2010. Trajectory 2005-2020 represents the emission scenarios for 2005 to 2020, assuming constant traffic volume and speed.

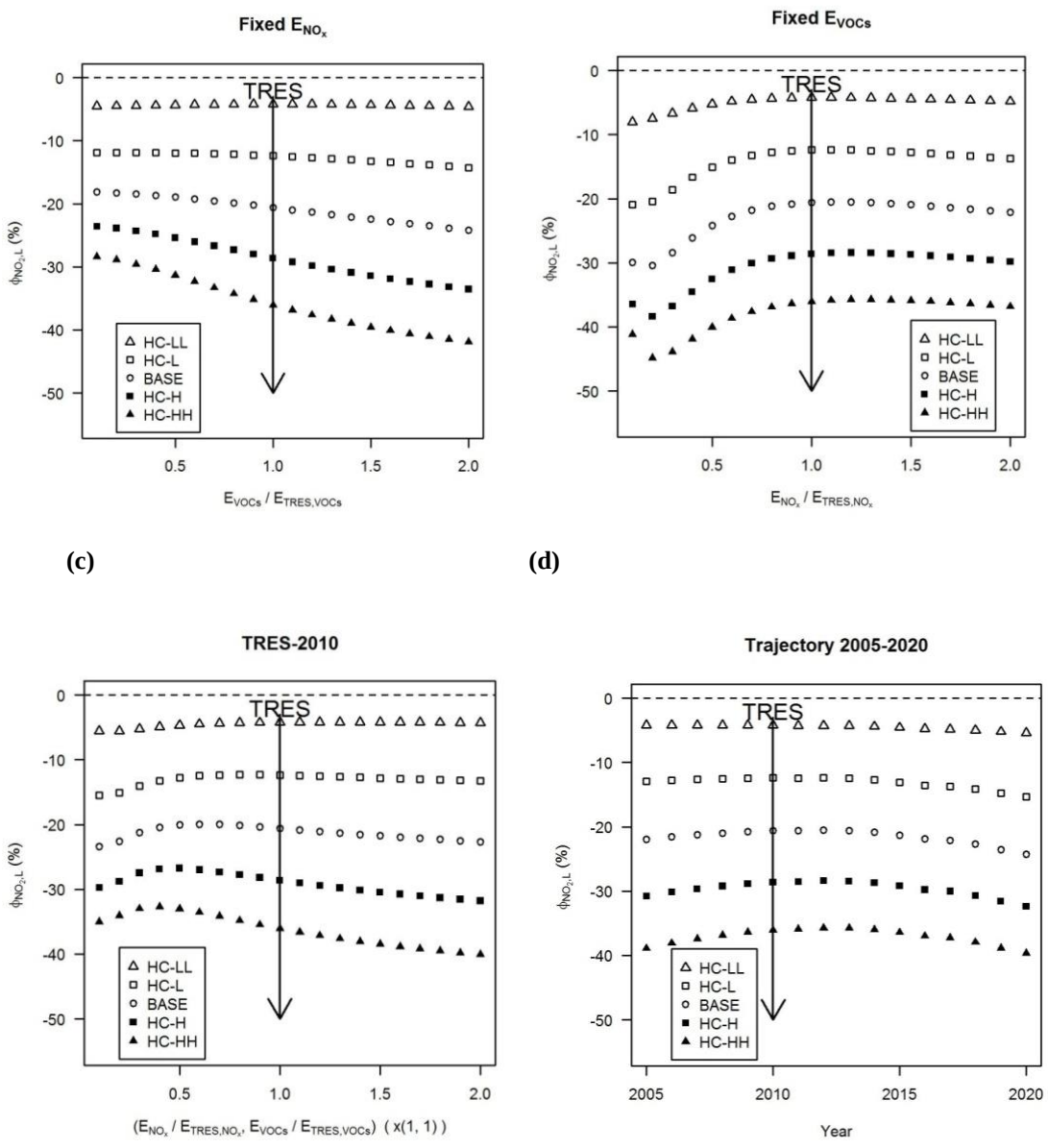

Figure 7 $\phi_{NO_2,L}$ (%), i.e. the percentage of overestimation for NO_2 in the lower canyon by the 'one-box' model compared with that by the "two-box" model, for (a) "Fixed E_{NOx}" at a fixed NO_x emissions of TRES, (b) "Fixed E_{VOCs}" at a fixed VOCs emissions of TRES, (c) "TRES-2010" varying the total traffic volume only and (d) "Trajectory 2005-2020" assuming constant traffic volume and speed varying η. E_{VOCs} and E_{NOx} are normalised by those of the Typical Real-world Emission Scenario (TRES, represented by△), for the year of 2010.

722 **(a)** **(b)**

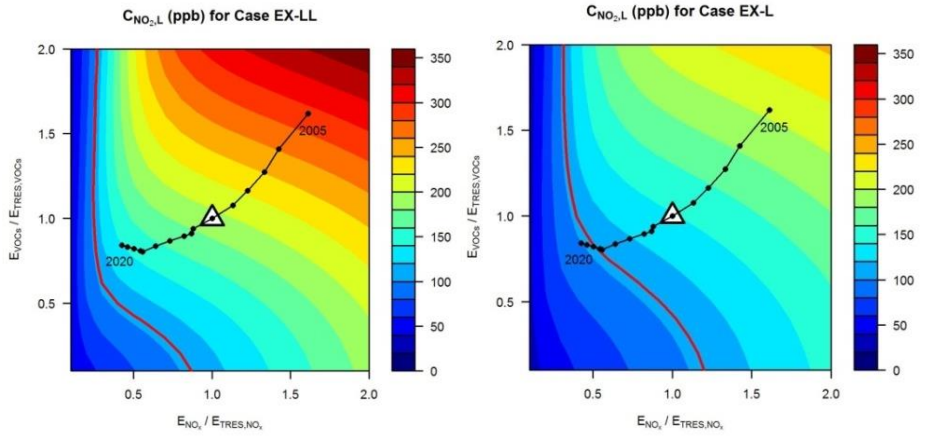

723

724 **(c)** **(d)**

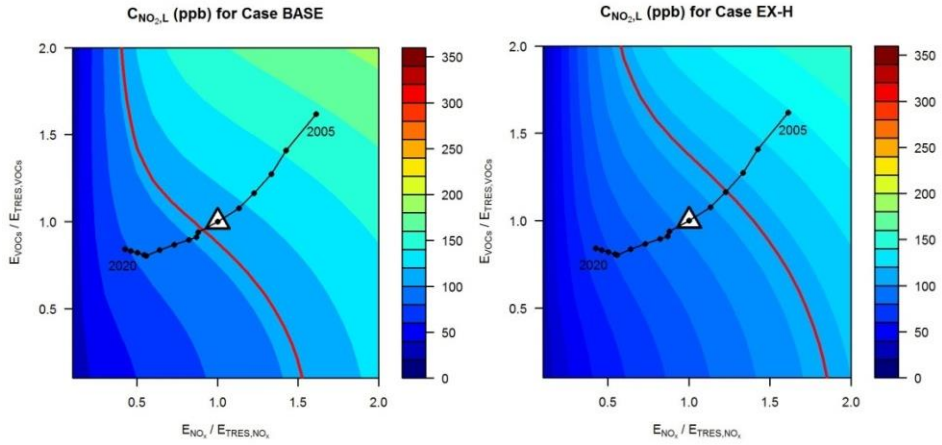

725

726 **(e)**

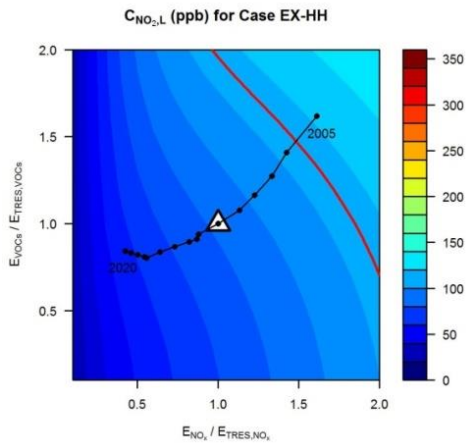

727

728 **Figure 8 $C_{NO_2,L}$ (ppb), i.e. the concentration in the lower box derived from the "two-box" model, in the (a) Case**
729 **EX-LL ($w_{t,0}$ =0.012 m s^{-1}), (b) Case EX-L ($w_{t,0}$ =0.016 m s^{-1}), (c) Case BASE ($w_{t,0}$ =0.02 m s^{-1}), (d) Case EX-**
730 **H ($w_{t,0}$ =0.024 m s^{-1}) and (e) Case EX-HH ($w_{t,0}$ =0.028 m s^{-1}). E_{VOCs} and E_{NOx} are normalised by those of the**
731 **Typical Real-world Emission Scenario (TRES, represented by△), for the year of 2010. Trajectory 2005-2020**
732 **represents the emission scenarios for 2005 to 2020, assuming constant traffic volume and speed. The solid red**
733 **curves denote the UK air quality standard for hourly NO_2 (105 ppb).**

734 **(a)** **(b)**

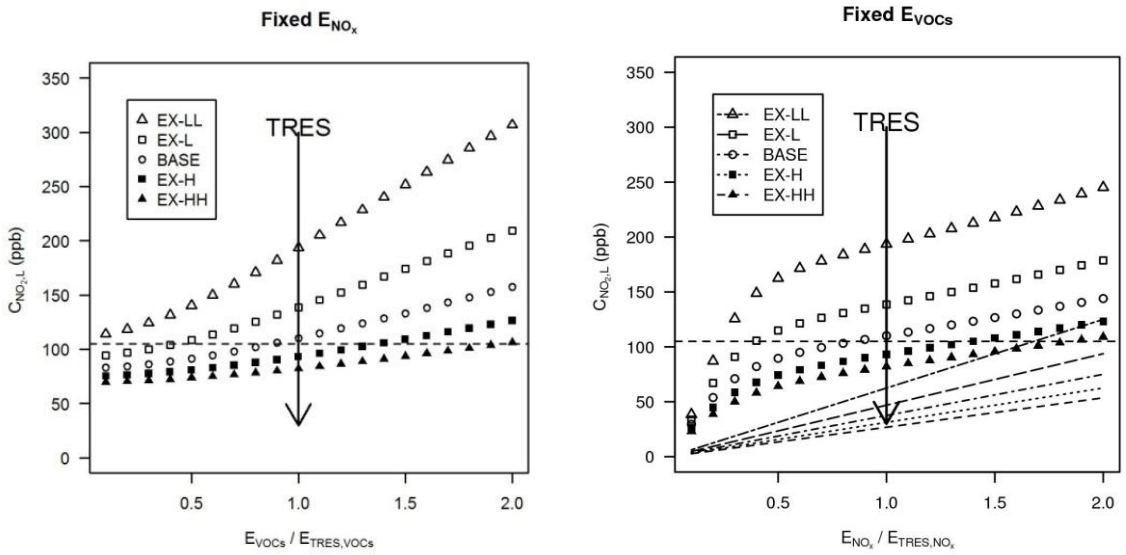

735

736 **(c)** **(d)**

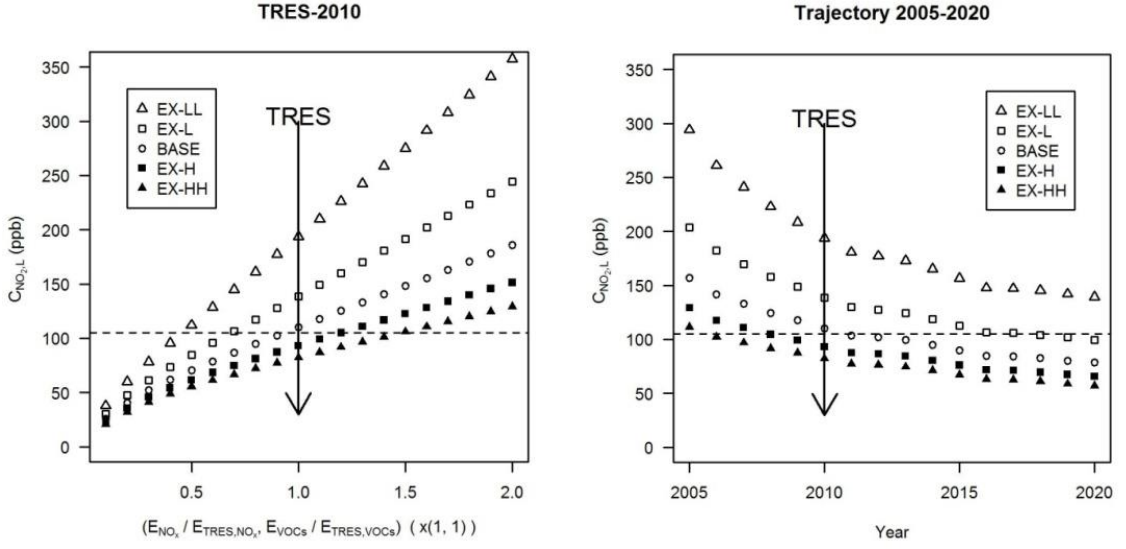

737

738 **Figure 9 $C_{NO_2,L}$ (ppb), i.e. the concentration in the lower box derived from the "two-box" model, for (a) "Fixed**
739 ***E*$_{NOx}$" at a fixed NO$_x$ emissions of TRES, (b) "Fixed *E*$_{VOCs}$" at a fixed VOCs emissions of TRES (The direct**
740 **contributions of NO$_x$ emissions to $C_{NO_2,L}$ are indicated by a series of radiating lines, running from highest to**
741 **lowest for the cases from EX-LL to HC-HH.), (c) "TRES-2010" varying the total traffic volume only and (d)**
742 **"Trajectory 2005-2020" assuming constant traffic volume and speed varying $w_{t,0}$. *E*$_{VOCs}$ and *E*$_{NOx}$ are**
743 **normalised by those of the Typical Real-world Emission Scenario (TRES, represented by△), for the year of**
744 **2010. The dashed line indicates the UK air quality standard for hourly NO$_2$ (105 ppb).**

745

746

747

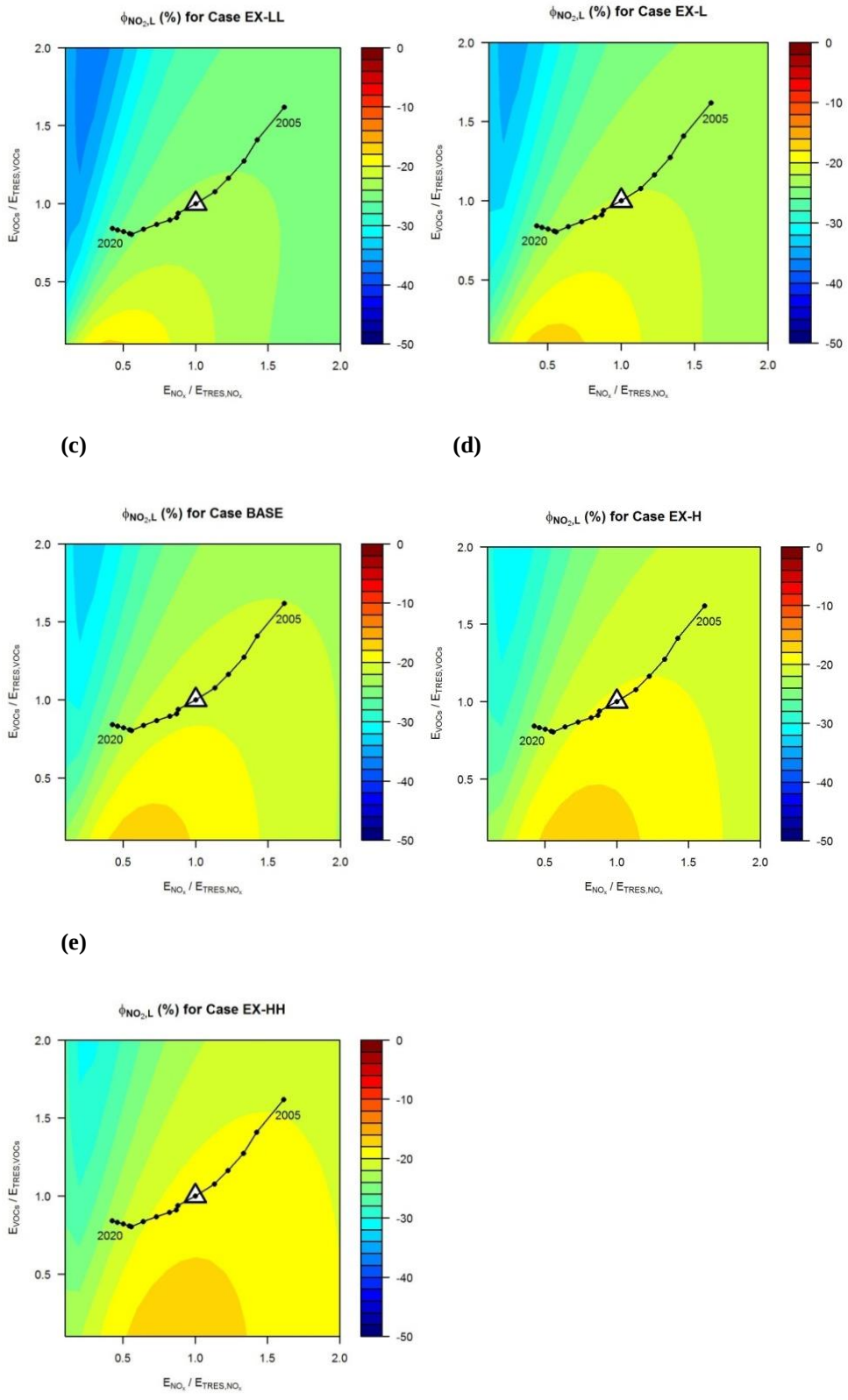

Figure 10 $\phi_{NO_2,L}$ (%), i.e. the percentage of overestimation for NO_2 in the lower canyon by the 'one-box' model compared with that by the "two-box" model, in the (a) Case EX-LL ($w_{t,0}$ =0.012 m s^{-1}), (b) Case EX-L ($w_{t,0}$ =0.016 m s^{-1}), (c) Case BASE ($w_{t,0}$ =0.02 m s^{-1}), (d) Case EX-H ($w_{t,0}$ =0.024 m s^{-1}) and (e) Case EX-HH ($w_{t,0}$ =0.028 m s^{-1}). E_{VOCs} and E_{NOx} are normalised by those of the Typical Real-world Emission Scenario (TRES, represented by△), for the year of 2010. Trajectory 2005-2020 represents the emission scenarios for 2005 to 2020, assuming constant traffic volume and speed.

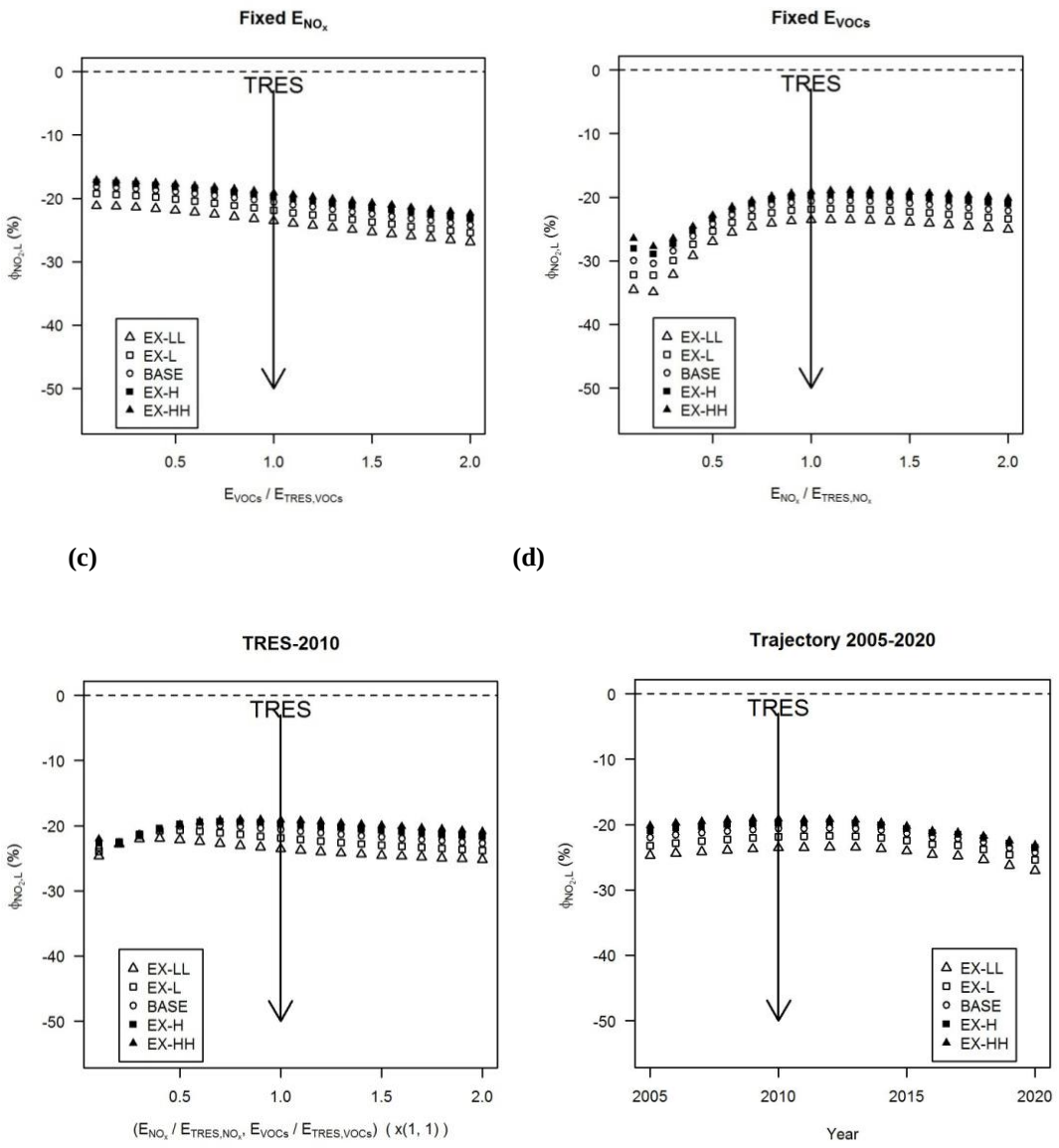

Figure 11 $\phi_{NO_2,L}$ (%), i.e. the percentage of overestimation for NO_2 in the lower canyon by the 'one-box' model compared with that by the "two-box" model, for (a) "Fixed E_{NOx}" at a fixed NO_x emissions of TRES, (b) "Fixed E_{VOCs}" at a fixed VOCs emissions of TRES, (c) "TRES-2010" varying the total traffic volume only and (d) "Trajectory 2005-2020" assuming constant traffic volume and speed varying $w_{t,0}$. E_{VOCs} and E_{NOx} are normalised by those of the Typical Real-world Emission Scenario (TRES, represented by△), for the year of 2010.

775

776 **(a)** **(b)**

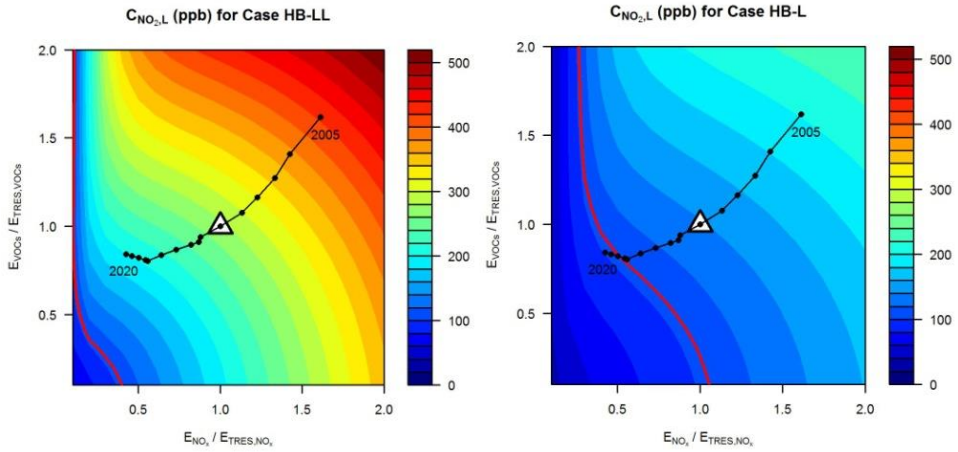

777

778 **(c)** **(d)**

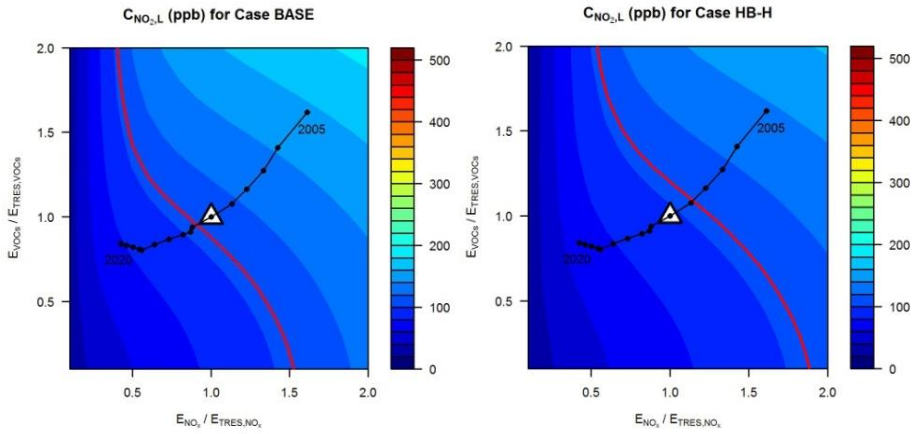

779

780 **(e)**

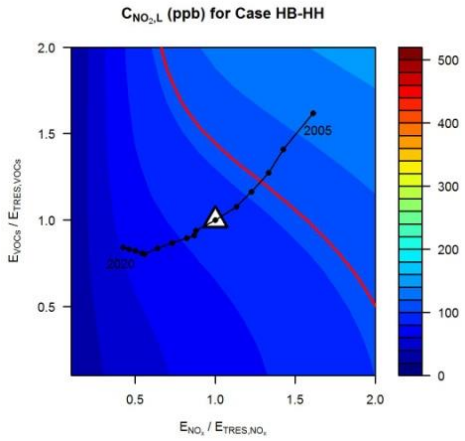

781

782 **Figure 12 $C_{NO_2,L}$ (ppb), i.e. the concentration in the lower box derived from the "two-box" model, in the (a) Case**
783 **HB-LL (α =0.1), (b) Case HB-L (α =0.3), (c) Case BASE (α =0.5), (d) Case HB-H (α =0.7), and (e) Case HB-**
784 **HH (α =0.9). E_{VOCs} and E_{NOx} are normalised by those of the Typical Real-world Emission Scenario (TRES,**
785 **represented by△), for the year of 2010. Trajectory 2005-2020 represents the emission scenarios for 2005 to 2020,**
786 **assuming constant traffic volume and speed. The solid red curves denote the UK air quality standard for hourly**
787 **NO_2 (105 ppb).**

788

789 **(a)** **(b)**

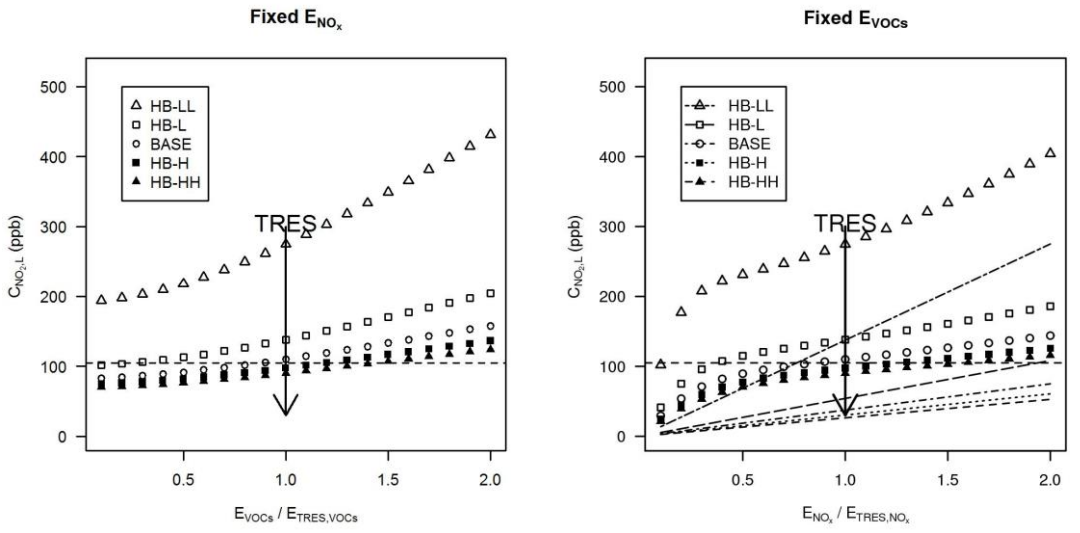

790

791 **(c)** **(d)**

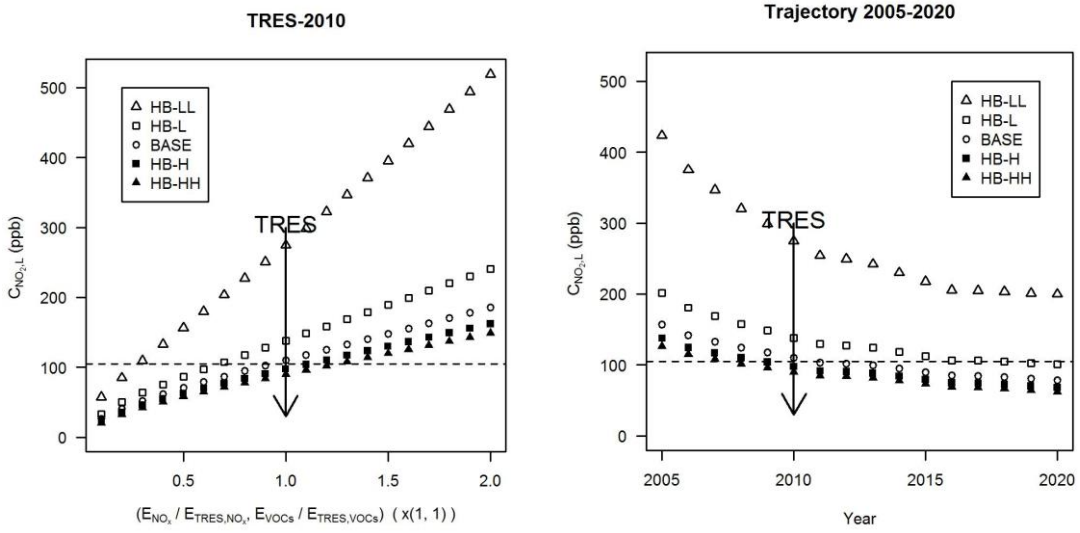

792

793 **Figure 13 $C_{NO_2,L}$ (ppb), i.e. the concentration in the lower box derived from the "two-box" model, for (a) "Fixed**
794 **E_{NOx}" at a fixed NO_x emissions of TRES, (b) "Fixed E_{VOCs}" at a fixed VOCs emissions of TRES (The direct**
795 **contributions of NO_x emissions to $C_{NO_2,L}$ are indicated by a series of radiating lines, running from highest to**
796 **lowest for the cases from HB-LL to HB-HH.), (c) "TRES-2010" varying the total traffic volume only and (d)**
797 **"Trajectory 2005-2020" assuming constant traffic volume and speed varying α. E_{VOCs} and E_{NOx} are normalised**
798 **by those of the Typical Real-world Emission Scenario (TRES, represented by△), for the year of 2010. The**
799 **dashed line indicates the UK air quality standard for hourly NO_2 (105 ppb).**

800

801

802

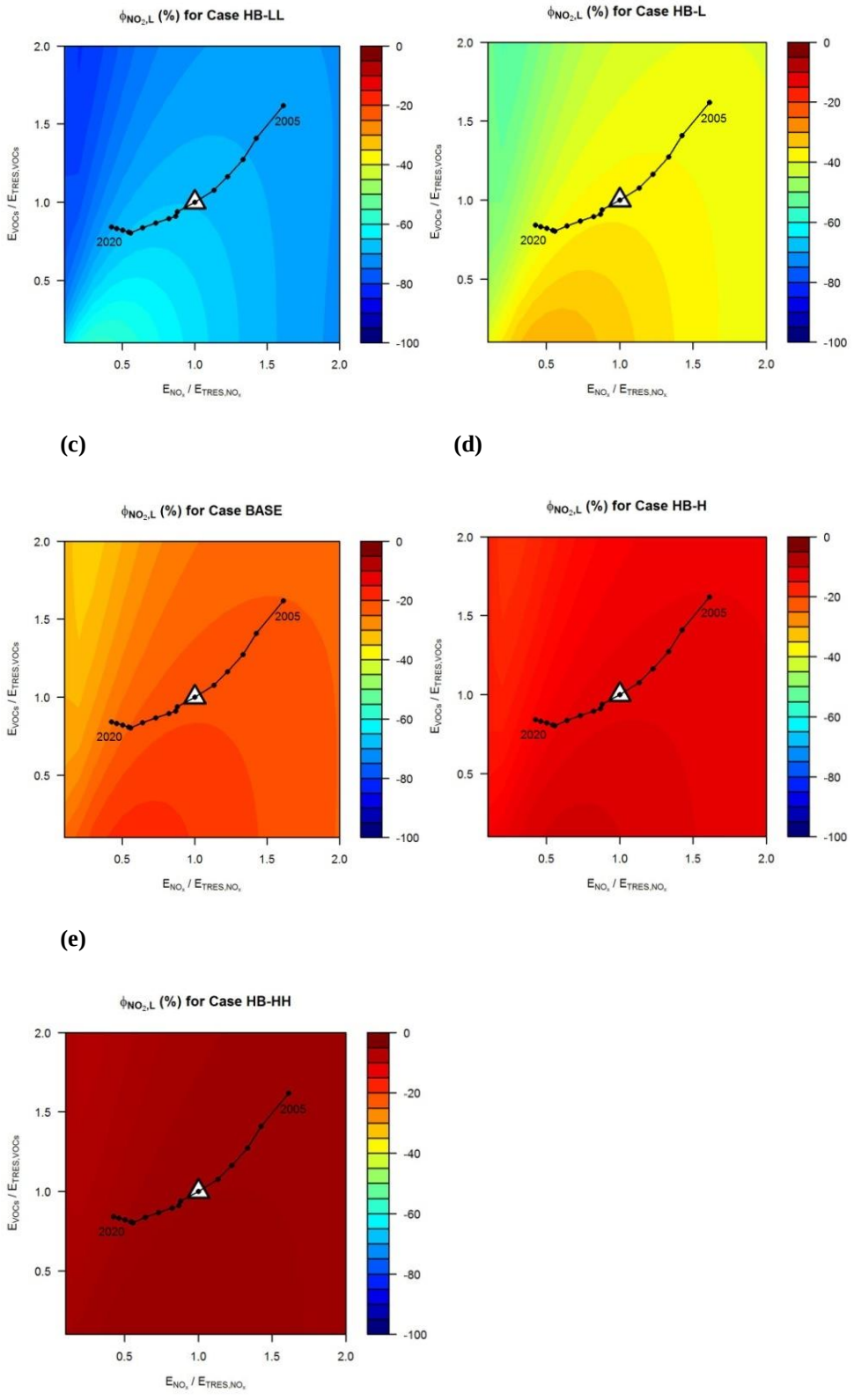

Figure 14 $\phi_{NO_2,L}$ (%), i.e. the percentage of overestimation for NO_2 in the lower canyon by the 'one-box' model compared with that by the "two-box" model, in the (a) Case HB-LL (α =0.1), (b) Case HB-L (α =0.3), (c) Case BASE (α =0.5), (d) Case HB-H (α =0.7), and (e) Case HB-HH (α =0.9). E_{VOCs} and E_{NOx} are normalised by those of the Typical Real-world Emission Scenario (TRES, represented by△), for the year of 2010. Trajectory 2005-2020 represents the emission scenarios for 2005 to 2020, assuming constant traffic volume and speed. The solid red curves denote the UK air quality standard for hourly NO_2 (105 ppb).

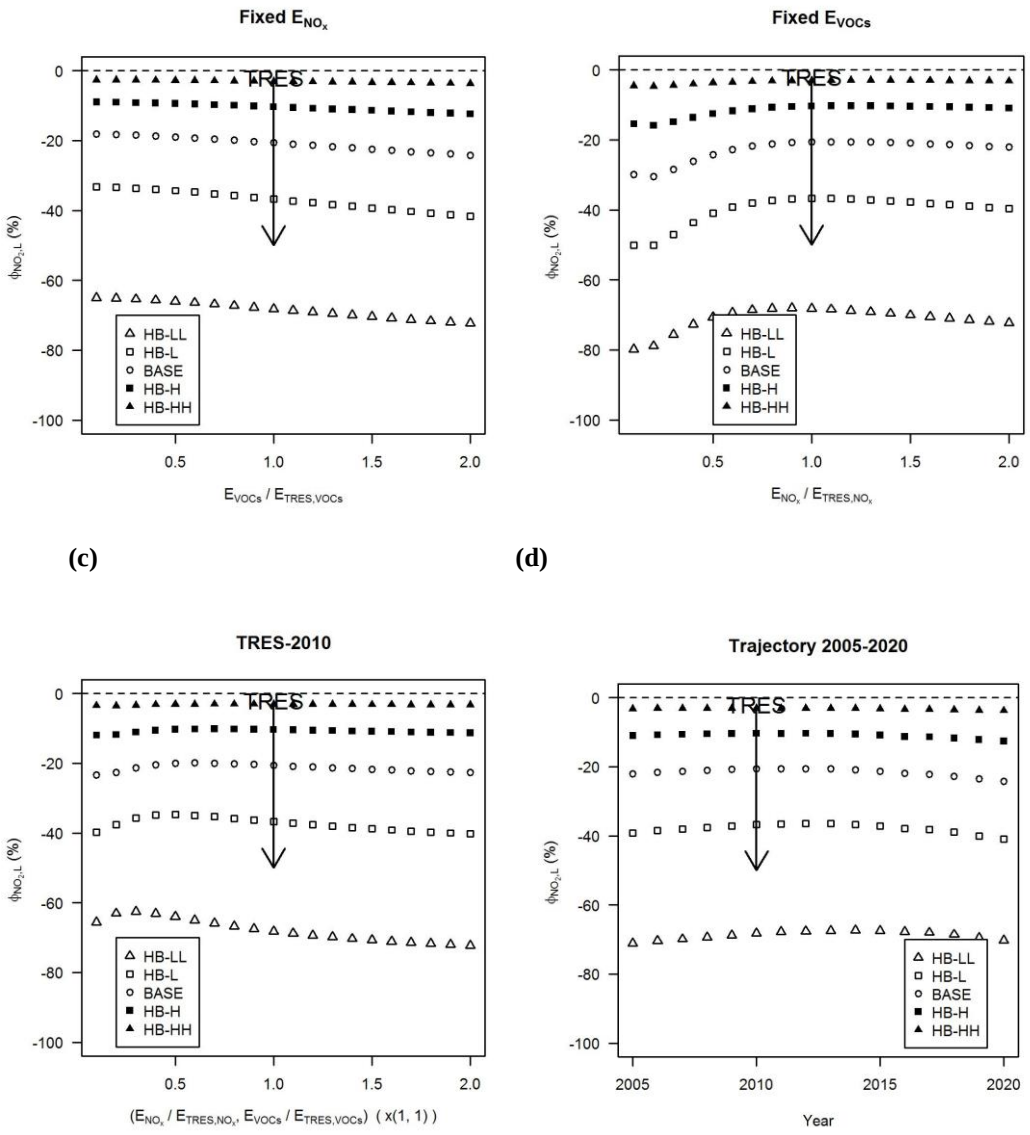

Figure 15 $\phi_{NO_2,L}$ (%), i.e. the percentage of overestimation for NO_2 in the lower canyon by the 'one-box' model compared with that by the "two-box" model, for (a) "Fixed E_{NOx}" at a fixed NO_x emissions of TRES, (b) "Fixed E_{VOCs}" at a fixed VOCs emissions of TRES, (c) "TRES-2010" varying the total traffic volume only and (d) "Trajectory 2005-2020" assuming constant traffic volume and speed varying α. E_{VOCs} and E_{NOx} are normalised by those of the Typical Real-world Emission Scenario (TRES, represented by△), for the year of 2010.

References:

BAKER, J., WALKER, H. L. & CAI, X. M. 2004. A study of the dispersion and transport of reactive pollutants in and above street canyons - a large eddy simulation. *Atmospheric Environment,* 38**,** 6883-6892.

BARLOW, J. F., HARMAN, I. N. & BELCHER, S. E. 2004. Scalar fluxes from urban street canyons. Part I: Laboratory simulation. *Boundary-Layer Meteorology,* 113**,** 369-385.

BOULTER, P. G., BARLOW, T. J., LATHAM, S. & MCCRAE, I. S. 2009. Emission Factors 2009: Report 1 - a review of methods for determining hot exhaust emission factors for road vehicles. *TRL: Wokingham*.

BRIGHT, V. B. 2013. *Street canyon atmospheric composition: coupling dynamics and chemistry.* Ph.D. thesis, University of Birmingham.

BRIGHT, V. B., BLOSS, W. J. & CAI, X. M. 2013. Urban street canyons: Coupling dynamics, chemistry and within-canyon chemical processing of emissions. *Atmospheric Environment,* 68**,** 127-142.

BUCKLAND, A. T. 1998. Validation of a street canyon model in two cities. *Environmental Monitoring and Assessment,* 52**,** 255-267.

CARSLAW, D. & RHYS-TYLER, G. 2013. Remote sensing of NO_2 exhaust emissions from road vehicles. *A report to the City of London Corporation and London Borough of Ealing*.

CATON, F., BRITTER, R. E. & DALZIEL, S. 2003. Dispersion mechanisms in a street canyon. *Atmospheric Environment,* 37**,** 693-702.

DEFRA 2008. The Air Quality Strategy for England, Scotland, Wales and Northern Ireland. Volume 1.

GROMKE, C. & RUCK, B. 2012. Pollutant Concentrations in Street Canyons of Different Aspect Ratio with Avenues of Trees for Various Wind Directions. *Boundary-Layer Meteorology,* 144**,** 41-64.

KWAK, K. H., BAIK, J. J. & LEE, K. Y. 2013. Dispersion and photochemical evolution of reactive pollutants in street canyons. *Atmospheric Environment,* 70**,** 98-107.

LI, X.-X., LIU, C.-H. & LEUNG, D. Y. C. 2008. Large-eddy simulation of flow and pollutant dispersion in high-aspect-ratio urban street canyons with wall model. *Boundary-Layer Meteorology,* 129**,** 249-268.

LI, X. X., BRITTER, R. E., NORFORD, L. K., KOH, T. Y. & ENTEKHABI, D. 2012. Flow and Pollutant Transport in Urban Street Canyons of Different Aspect Ratios with Ground Heating: Large-Eddy Simulation. *Boundary-Layer Meteorology,* 142**,** 289-304.

LI, X. X., LIU, C. H. & LEUNG, D. Y. C. 2009. Numerical investigation of pollutant transport characteristics inside deep urban street canyons. *Atmospheric Environment,* 43**,** 2410-2418.

LIU, C.-H., CHENG, W. C., LEUNG, T. C. Y. & LEUNG, D. Y. C. 2011. On the mechanism of air pollutant re-entrainment in two-dimensional idealized street canyons. *Atmospheric Environment,* 45**,** 4763-4769.

LIU, C.-H. & LEUNG, D. Y. C. 2008. Numerical study on the ozone formation inside street canyons using a chemistry box model. *Journal of Environmental Sciences-China,* 20**,** 832-837.

LIU, C. H., LEUNG, D. Y. C. & BARTH, M. C. 2005. On the prediction of air and pollutant exchange rates in street canyons of different aspect ratios using large-eddy simulation. *Atmospheric Environment,* 39**,** 1567-1574.

LOUKA, P., BELCHER, S. E. & HARRISON, R. G. 2000. Coupling between air flow in streets and the well-developed boundary layer aloft. *Atmospheric Environment,* 34**,** 2613-2621.

MURENA, F. 2012. Monitoring and modelling carbon monoxide concentrations in a deep street canyon: application of a two-box model. *Atmospheric Pollution Research,* 3**,** 311-316.

MURENA, F., DI BENEDETTO, A., D'ONOFRIO, M. & VITIELLO, G. 2011. Mass Transfer Velocity and Momentum Vertical Exchange in Simulated Deep Street Canyons. *Boundary-Layer Meteorology,* 140**,** 125-142.

MURENA, F. & FAVALE, G. 2007. Continuous monitoring of carbon monoxide in a deep street canyon. *Atmospheric Environment,* 41**,** 2620-2629.
MURENA, F., FAVALE, G., VARDOULAKIS, S. & SOLAZZO, E. 2009. Modelling dispersion of traffic pollution in a deep street canyon: Application of CFD and operational models. *Atmospheric Environment,* 43**,** 2303-2311.
MURENA, F., GAROFALO, N. & FAVALE, G. 2008. Monitoring CO concentration at leeward and windward sides in a deep street canyon. *Atmospheric Environment,* 42**,** 8204-8210.
NAEI 2003. UK fleet composition projections. *URL: http://naei.defra.gov.uk/data/ef-transport*.
OKE, T. R. 1987. Boundary Layer Climates. *second ed,* Methuen**,** London.
PUGH, T. A. M., MACKENZIE, A. R., WHYATT, J. D. & HEWITT, C. N. 2012. Effectiveness of Green Infrastructure for Improvement of Air Quality in Urban Street Canyons. *Environmental Science & Technology,* 46**,** 7692-7699.
RAMAMURTHY, P., PARDYJAK, E. R. & KLEWICKI, J. C. 2007. Observations of the effects of atmospheric stability on turbulence statistics deep within an urban street canyon. *Journal of Applied Meteorology and Climatology,* 46**,** 2074-2085.
SAHM, P., LOUKA, P., KETZEL, M., GUILLOTEAU, E. & SINI, J. F. 2002. *Intercomparison of numerical urban dispersion models - Part I: Street canyon and single building configurations*.
SALIM, S. M., BUCCOLIERI, R., CHAN, A. & DI SABATINO, S. 2011. Numerical simulation of atmospheric pollutant dispersion in an urban street canyon: Comparison between RANS and LES. *Journal of Wind Engineering and Industrial Aerodynamics,* 99**,** 103-113.
SALIZZONI, P., SOULHAC, L. & MEJEAN, P. 2009. Street canyon ventilation and atmospheric turbulence. *Atmospheric Environment,* 43**,** 5056-5067.
ZHONG, J., CAI, X. & BLOSS, W. J. 2014. Modelling segregation effects of heterogeneous emissions on ozone levels in idealised urban street canyons: Using photochemical box models *Environmental Pollution,* 188**,** 132-143.
ZHONG, J., CAI, X. & BLOSS, W. J. 2015. Modelling the dispersion and transport of reactive pollutants in a deep urban street canyon: Using large-eddy simulation. *Environmental Pollution,* 200**,** 42-52.
ZHONG, J., CAI, X. & BLOSS, W. J. 2016. Coupling dynamics and chemistry in the air pollution modelling of street canyons: A review. *Environmental Pollution,* 214**,** 690–704.